Advances in Computational Mathematics https://doi.org/10.1007/s10444-019-09739-0

Commutation error in reduced order modeling of fluid flows



Birgul Koc¹ · Muhammad Mohebujiaman² · Changhong Mou¹ · Trajan Iljescu¹

Received: 1 October 2018 / Accepted: 3 October 2019 / Published online: 09 December 2019 © Springer Science+Business Media, LLC, part of Springer Nature 2019

Abstract

For reduced order models (ROMs) of fluid flows, we investigate theoretically and computationally whether differentiation and ROM spatial filtering commute, i.e., whether the commutation error (CE) is nonzero. We study the CE for the Laplacian and two ROM filters: the ROM projection and the ROM differential filter. Furthermore, when the CE is nonzero, we investigate whether it has any significant effect on ROMs that are constructed by using spatial filtering. As numerical tests, we use the Burgers equation with viscosities $v = 10^{-1}$ and $v = 10^{-3}$ and a 2D flow past a circular cylinder at Reynolds numbers Re = 100 and Re = 500. Our investigation (i) measures the size of the CE in these test problems and (ii) shows that the CE has a significant effect on ROM development for high viscosities, but not so much for low viscosities.

Keywords Reduced order model · Spatial filter · Commutation error · Data-driven model

Mathematics Subject Classification (2010) 65M60 · 76F65

1 Introduction

1.1 Motivation and prior work

Reduced order models (ROMs) [11, 15, 34] have been used for decades in the numerical simulation of fluid flows [2, 4, 14, 16, 27, 40, 41]. If the ROM dimension is

Communicated by: Anthony Nouy

Changhong Mou and Traian Iliescu are partially supported by DMS-1821145

 □ Birgul Koc
 □ birgul@vt.edu

Extended author information available on the last page of the article.



high enough to capture the relevant flow features, ROMs yield efficient and relatively accurate approximations of the underlying flows. However, to ensure a low computational cost, the ROM dimension is often lower than the dimension required by an accurate numerical simulation. This happens, for example, in turbulent flows, where the ROM dimension is generally significantly lower than the dimension needed to capture all the relevant flow features [8, 9, 12, 16, 30, 39]. In these challenging simulations, the low dimensional ROMs often yield inaccurate results. The general explanation for these inaccurate results is that the ROMs fail to account for the interaction between the resolved ROM modes and the unresolved ROM modes that are discarded in the often drastic ROM truncation [9, 13, 28, 29, 42, 44, 45]. Thus, when the ROM dimension is too low to capture the relevant flow features, ROMs are generally supplemented with a *Correction term* [1, 3, 12, 13, 16, 21, 27, 30, 37, 42].

In our recent work [44], we have shown that this Correction term can be explicitly calculated and modeled with the available data by using the ROM projection as a ROM spatial filter. (In Section 3.1, we present two examples of ROM spatial filters: the ROM differential filter and the ROM projection filter.) We note that ROM spatial filtering has also been used to develop large eddy simulation ROMs, e.g., approximate deconvolution ROMs [45] and eddy viscosity ROMs [3, 16, 27, 33, 36, 42]. In all these ROMs, it has been been assumed that differentiation and ROM spatial filtering commute:

$$\frac{\partial u}{\partial x} = \frac{\partial \overline{u}}{\partial x},\tag{1}$$

where u is a flow variable (such as a component of the velocity field $u \in X = H_0^1(\Omega)$ in the Navier-Stokes equations (4)–(5)) and x is a spatial direction.

1.2 Problem formulation and contributions

In this paper, we investigate theoretically and numerically whether there exists a *commutation error (CE)*, i.e., whether equality (1) holds. At an abstract level, it seems that the CE (1) is generally nonzero. Indeed, imagine a simple one-dimensional example in which the ROM basis functions are constants and consider the ROM projection filter (defined in Section 3.1) as a spatial filter. In this case, the right-hand side of (1) is zero and the left-hand side of (1) is generally nonzero, i.e., the CE exists.

In this paper we investigate the CE theoretically (for general ROM settings) and numerically (for two test problems).

In particular, we investigate whether there is a CE for the Laplacian, which plays a central role in fluid dynamics:

$$\overline{\Delta u} = \Delta \overline{u}.\tag{2}$$

Remark 1 (ROM Closure) It is well known that, in general, nonlinearity and ROM spatial filtering do *not* commute:

$$\overline{\mathcal{N}(u)} \neq \mathcal{N}(\overline{u}),\tag{3}$$



where u is a flow variable and \mathcal{N} is a nonlinear term in the underlying equations. Furthermore, in ROMs for nonlinear convection-dominated flows, the difference between the two terms in (3) is generally significant and needs to be modeled for accurate approximations. The resulting models are called *ROM closure models* [42, 44].

We emphasize that the CE in (1) is different from the closure problem in (3). Indeed, the former quantifies the effect of interchanging the order of spatial differentiation and ROM spatial filtering, whereas the latter quantifies the effect of interchanging the order of nonlinear operations (e.g., multiplication) and ROM spatial filtering.

We also emphasize that, in this paper, we do *not* focus on the development of ROM closure models, which have been investigated in numerous studies, e.g., [1, 3, 12, 13, 16, 21, 27, 30, 37, 42, 44]. Instead, we investigate whether the CE is an important component of the "correct" ROM closure model, i.e., whether the CE should complement (not replace) current ROM closure models. To our knowledge, this study represents the first explicit numerical investigation of the CE in a ROM context.

When the CE exists, we also investigate whether it has any significant effect on the ROM itself. To this end, we consider the recently proposed *data-driven correction ROM (DDC-ROM)* [44], in which the Correction term (which is generally added to improve the ROM's accuracy) is modeled using the available data [7, 23, 24, 31, 32]. To investigate the effect of the CE on the DDC-ROM by using the metric (51), we also consider the *commutation error DDC-ROM (CE-DDC-ROM)*, in which available data is used to model not only the Correction term, but also the CE. Finally, we use the *ideal CE-DDC-ROM (ICE-DDC-ROM)*, which is the DDC-ROM supplemented with a fine resolution representation (i.e., without any additional modeling) of the CE. When the CE-DDC-ROM and the ICE-DDC-ROM yield more accurate results than the standard DDC-ROM, we conclude that the CE has a significant effect on the DDC-ROM and, therefore, should be modeled. As numerical tests, we use the Burgers equation with viscosities $\nu = 10^{-1}$ and $\nu = 10^{-3}$ and a 2D flow past a circular cylinder at Reynolds numbers Re = 100 and Re = 500.

The tests that we use in our numerical investigation are relatively simple. In these settings, standard ROMs can yield relatively accurate approximations if a sufficient number of ROM basis functions are used, in which case ROM closure modeling (i.e., adding a Correction term) is not actually needed. We emphasize, however, that when only a few ROM basis functions are used, using ROM closure modeling can improve the ROM accuracy even in these relatively simple settings. In these cases, the study of the CE becomes relevant. We also note that in this paper we do *not* focus on the development of ROM closure models. Instead, we aim at discovering whether the CE is a significant component of ROM closure models. As a first step in our CE numerical investigation, we used relatively simple test problems. Of course, in future studies we will investigate ROM closure models that integrate all the components and we will test them in more challenging, realistic computational settings that require a drastic ROM truncation [30, 42].



1.3 Paper plan

The paper is organized as follows: The reduced order modeling preliminaries are provided in Section 2. In Section 3, a detailed derivation of the CE is given. The effects of the CE on ROMs that are constructed by using spatial filtering are discussed in Section 4. Numerical experiments are given in Section 5, and conclusions and future research directions are outlined in Section 6.

2 Reduced order modeling

To compute the ROM basis functions, we use the proper orthogonal decomposition (POD) [10, 16, 27], which we briefly describe in this section. We emphasize, however, that our theoretical and computational developments carry over to other ROM basis functions, such as the dynamic mode decomposition [38]. The snapshots $\{u_h^1, u_h^2, \cdots, u_h^M\}$ are the finite element (FE) solutions of at M different time instances. The POD seeks a low-dimensional basis that approximates the snapshots optimally with respect to a certain norm. The commonly used L^2 norm will be used in this paper. We emphasize, however, that other norms could be used to construct the POD basis [17]. The solution of the minimization problem is equivalent to the solution of the eigenvalue problem $\frac{1}{M}YY^TM_h\phi_j=\lambda_j\phi_j, j=1,\cdots,N_h$, where ϕ_j and λ_i denote the vector of the FE coefficients of the POD basis functions and the POD eigenvalues, respectively, Y denotes the snapshot matrix, whose columns correspond to the FE coefficients of the snapshots, M_h represents the FE mass matrix, and N_h is the dimension of the FE space X^h . The eigenvalues are real and non-negative, so they can be ordered as follows: $\lambda_1 \geq \lambda_2 \geq \cdots \geq \lambda_d > \lambda_{d+1} = \cdots = \lambda_{N_h} = 0$, where d is the rank of the snapshot matrix Y. The ROM basis is given by the normalized vectors $\{\phi_j\}_{j=1}^r$, which correspond to the first $r \leq N_h$ largest eigenvalues. Thus, the ROM space is defined as $X^r := \text{span}\{\phi_1, \phi_2, \cdots, \phi_r\}$.

3 Commutation error

As a mathematical model, we consider the incompressible time-dependent Navier-Stokes equations (NSE):

$$\frac{\partial \mathbf{u}}{\partial t} - \nu \Delta \mathbf{u} + \mathbf{u} \cdot \nabla \mathbf{u} + \nabla p = \mathbf{0} \ \Omega \times (0, T], \tag{4}$$

$$\nabla \cdot \boldsymbol{u} = 0 \ \Omega \times (0, T], \tag{5}$$

$$\mathbf{u} = 0 \ \partial \Omega \times (0, T), \tag{6}$$

where u is the velocity, p the pressure, v the kinematic viscosity, T the simulation time, and Ω the domain of the fluid. We use the initial condition $u(\mathbf{x}, 0) = u_0(\mathbf{x})$. In this paper, we assume that $\Omega \subset \mathbb{R}^n$, $n \in \{2, 3\}$, is a convex polygonal or polyhedron domain with boundary $\partial \Omega$. The discrete FE velocity and pressure spaces are denoted by $X^h \subset X = H_0^1(\Omega)$ and $Q^h \subset Q = L^2(\Omega)$, respectively. We denote the usual



 $L^2(\Omega)$ norm and inner product with $\|\cdot\|$ and (\cdot, \cdot) , respectively. To derive the commutation error due to filtering, we apply a continuous filter [5] to (4). Discrete ROM spatial filters are introduced in Section 3.1.

This yields the filtered-NSE (F-NSE), which have been used to develop LES models [5]:

$$\frac{\partial u}{\partial t} - \nu \overline{\Delta u} + \overline{(u \cdot \nabla)u} + \overline{\nabla p} = \mathbf{0}. \tag{7}$$

The F-NSE (7) eliminate the small length scales in the continuous NSE (4). For this reason, a ROM for (7) needs fewer POD modes than a ROM for (4) to achieve a fixed numerical accuracy. However, to develop practical ROMs for the F-NSE (7), we must first investigate the commutation error, i.e., whether filtering and differentiation commute. The *commutation error* (CE) for a spatial derivative is defined in [5] as

$$\mathcal{E}_{k}[\boldsymbol{u}](\mathbf{x}) := \frac{\partial \overline{\boldsymbol{u}}(\mathbf{x})}{\partial x_{k}} - \frac{\overline{\partial \boldsymbol{u}(\mathbf{x})}}{\partial x_{k}}, \tag{8}$$

where $\mathbf{x} = [x_1, \dots, x_n]$ is the spatial variable. In this paper, we are particularly interested in the CE for the Laplacian term. Similarly to (8), we define the Laplacian CE as

$$\mathcal{E}_{\Lambda}[u](\mathbf{x}) := \Delta \overline{u(\mathbf{x})} - \overline{\Delta u(\mathbf{x})}. \tag{9}$$

3.1 ROM spatial filter

To develop practical ROMs from the F-NSE (7), we need to replace the continuous filter in (7) with discrete filters. In this paper, we use the ROM differential filter (which is associated with a weighted H^1 projection) and the ROM projection filter (which is associated with the L^2 projection).

The *ROM differential filter (DF)* [43] is defined as: Let δ be radius of DF; for fixed $r \leq d$ and given $\boldsymbol{u}_d \in X^h$, the differential filter seeks $\overline{\boldsymbol{u}_d}^{DF} \in X^r$ such that

$$\left(\left(I - \delta^2 \Delta\right) \overline{\boldsymbol{u}_d}^{DF}, \boldsymbol{\phi}_i\right) = \left(\boldsymbol{u}_d, \boldsymbol{\phi}_i\right), \qquad \forall i = 1, ..., r.$$
 (10)

By using ROM approximations for both $\overline{u_d}^{DF}$ and u_d , i.e., $\overline{u_d}^{DF} = \sum_{j=1}^r (a_r)_j \phi_j$,

 $\mathbf{u}_d = \sum_{j=1}^d (\mathbf{a}_d)_j \boldsymbol{\phi}_j$, we obtain the following linear system:

$$\left(M_r + \delta^2 S_r\right) a_r = M_{r \times d} a_d, \tag{11}$$

where $M_r = (\phi_i, \phi_j)$, i, j = 1, ..., r and $M_{r \times d} = (\phi_i, \phi_j)$ i = 1, ..., r, j = 1, ..., d, are ROM mass matrices, $S_r = (\nabla \phi_i, \nabla \phi_j)$, i, j = 1, ..., r, is the ROM stiffness matrix, and a_r and a_d represent coefficient vectors of $\overline{u_d}^{DF}$ and u_d , respectively.

For fixed $r \leq d$ and given $u_d \in X^h$, the *ROM projection filter* [29, 42] seeks $\overline{u_d}^r \in X^r$ such that

$$\left(\overline{\boldsymbol{u}_d}^r, \boldsymbol{\phi}_i\right) = \left(\boldsymbol{u}_d, \boldsymbol{\phi}_i\right), \quad \forall i = 1, ...r.$$
 (12)

By expanding $\overline{u_d}^r$ and u_d in terms of the ROM basis, we obtain the following linear system:

$$M_r a_r = M_{r \times d} a_d, \tag{13}$$

where a_r and a_d are the coefficient vectors of $\overline{u_d}^r$ and u_d , respectively.

3.2 Filtered-ROM

In Section 3.1, we defined two ROM spatial filters: the ROM differential filter and the ROM projection filter. In this section, we take another step in the development of practical ROMs from the F-NSE (7). We assume that filtering and differentiation commute and replace the continuous velocity u in (7) with its most accurate approx-

imation in the snapshot space, i.e., with $u_d = \sum_{i=1}^d (a_d)_i \phi_j$, where d is the rank of the snapshot matrix: $\forall i = 1, ..., r$,

$$\left(\frac{\partial \overline{u_d}}{\partial t}, \phi_i\right) - \nu(\Delta \overline{u_d}, \phi_i) + ((\overline{u_d} \cdot \nabla) \overline{u_d}, \phi_i) + \tau_i = 0, \tag{14}$$

where

$$\tau_i = -\left(\boldsymbol{\tau}_d^{SFS}, \boldsymbol{\phi}_i\right),\tag{15}$$

$$\boldsymbol{\tau}_d^{SFS} = (\overline{\boldsymbol{u}_d} \cdot \nabla) \overline{\boldsymbol{u}_d} - \overline{(\boldsymbol{u}_d \cdot \nabla) \boldsymbol{u}_d}. \tag{16}$$

The filter $\overline{}$ in the *ROM subfilter-scale stress tensor* τ_d^{SFS} is either $\overline{}^r$ (i.e., the ROM projection filter (12)) or $\overline{}^{DF}$ (i.e., the ROM differential filter (10)).

We note that (14)–(16) is an r-dimensional system for the unknown $\overline{u_d} \in X^r$. For clarity, we denote the unknown $\overline{u_d}$ as

$$\overline{\boldsymbol{u}_d} := \boldsymbol{u}_r = \sum_{i=1}^r (\boldsymbol{a}_r)_i \boldsymbol{\phi}_i. \tag{17}$$

Using (17) in (14)–(16), we get: $\forall i = 1, ..., r$,

$$\left(\frac{\partial \boldsymbol{u}_r}{\partial t}, \boldsymbol{\phi}_i\right) + \nu(\nabla \boldsymbol{u}_r, \nabla \boldsymbol{\phi}) + ((\boldsymbol{u}_r \cdot \nabla)\boldsymbol{u}_r, \boldsymbol{\phi}_i) + \tau_i = 0, \tag{18}$$

where

$$\tau_i = -(\tau_r^{SFS}, \phi_i), \tag{19}$$

$$\tau_r^{SFS} = (u_r \cdot \nabla) u_r - \overline{(u_d \cdot \nabla) u_d}. \tag{20}$$

$$\boldsymbol{\tau}_r^{SFS} = (\boldsymbol{u}_r \cdot \nabla) \boldsymbol{u}_r - \overline{(\boldsymbol{u}_d \cdot \nabla) \boldsymbol{u}_d}. \tag{20}$$

Since (18) does not depend only on u_r , it is not a closed system. To close it, we need to solve the ROM *closure problem*, i.e., we need to find $\overline{(u_d \cdot \nabla)u_d} = f(u_r)$. Once a ROM closure model is found, the large eddy simulation ROM (LES-ROM) (14)–(16) becomes practical. The most commonly used ROM closure models have been of eddy viscosity type [42]. Alternative ROM closure models, inspired from image processing and inverse problems (i.e., the approximate deconvolution ROM [45]) and data-driven modeling (i.e., the data-driven correction ROM [44]) have been recently proposed. We emphasize that all these LES-ROMs assume that filtering and differentiation commute. In what follows, we investigate this assumption.



3.3 CE with differential filter

By using the ROM differential filter, the Laplacian CE in (9) can be written as:

$$\mathcal{E}_{\Delta}[\mathbf{u}_d] := \Delta \overline{\mathbf{u}_d}^{DF} - \overline{\Delta \mathbf{u}_d}^{DF}, \tag{21}$$

where $\overline{}^{DF}$ represents the ROM differential filter. We denote with \boldsymbol{a}_r , \boldsymbol{a}_d , \boldsymbol{b}_r and \boldsymbol{c}_r the coefficient vectors of $\overline{\boldsymbol{u}_d}^{DF}$, \boldsymbol{u}_d , $\Delta \overline{\boldsymbol{u}_d}^{DF}$, and $\overline{\Delta \boldsymbol{u}_d}^{DF}$, respectively. We start by evaluating $\Delta \overline{\boldsymbol{u}_d}^{DF}$:

$$(\Delta \overline{\boldsymbol{u}_d}^{DF}, \boldsymbol{\phi}_i) = -(\nabla \overline{\boldsymbol{u}_d}^{DF}, \nabla \boldsymbol{\phi}_i), \quad \forall i = 1, ..., r.$$
 (22)

Its corresponding linear system is

$$M_r \, \boldsymbol{b}_r = -S_r \, \boldsymbol{a}_r. \tag{23}$$

Using (11) and (23) gives

$$\mathbf{b}_r = -M_r^{-1} S_r (M_r + \delta^2 S_r)^{-1} M_{r \times d} \, \mathbf{a}_d. \tag{24}$$

Next, we evaluate $\overline{\Delta u_d}^{DF}$. Using equation (10), we write the following equation for $\overline{\Delta u_d}^{DF}$:

$$((I - \delta^2 \Delta) \overline{\Delta u_d}^{DF}, \boldsymbol{\phi}_i) = (\Delta u_d, \boldsymbol{\phi}_i), \quad \forall i = 1, ..., r.$$
 (25)

Its corresponding linear system is

$$(M_r + \delta^2 S_r) c_r = -S_{r \times d} a_d, \tag{26}$$

which yields

$$c_r = -(M_r + \delta^2 S_r)^{-1} S_{r \times d} \ a_d. \tag{27}$$

We note that the right hand sides of equations (24) and (27) are not equal. This suggests that, in some cases, for the ROM differential filter, the Laplacian CE can be nonzero:

$$\mathcal{E}_{\Delta}[\boldsymbol{u}_d] = \sum_{j=1}^{r} (\mathbf{b_r} - \mathbf{c_r})_j \boldsymbol{\phi}_j \neq 0.$$
 (28)

In the tests used in the numerical investigation in Section 5, the Laplacian CE is nonzero (see, e.g., Tables 1, 5, 9, 13, and 17.)

We also note that the vectors $\mathbf{b_r}$ and $\mathbf{c_r}$, which are needed in the calculation of the Laplacian CE in (28), are the solutions of the linear systems (24) and (27), respectively. These linear systems involve only the ROM mass matrices M_r and $M_{r \times d}$ and the ROM stiffness matrices S_r and $S_{r \times d}$, which can be computed with low order finite element discretizations, such as those that we use in Section 5.

3.4 CE with projection filter

By using the ROM projection filter, the Laplacian CE in (9) can be written as

$$\mathcal{E}_{\Delta}[\mathbf{u}_d] := \Delta \overline{\mathbf{u}_d}^r - \overline{\Delta \mathbf{u}_d}^r, \tag{29}$$



r	δ	$ \mathcal{E}_{\Delta}[u_d] _{L^2(L^2)}$	r	δ	$ \mathcal{E}_{\Delta}[u_d] _{L^2(L^2)}$
2	1.00e-01	1.40 <i>e</i> +00	5	1.00e-01	1.37 <i>e</i> +00
2	1.00e - 02	1.56e - 01	5	1.00e - 02	$8.98e{-02}$
2	1.00e - 03	1.53e - 01	5	1.00e - 03	1.26e - 03
2	1.00e - 04	1.54e - 01	5	1.00e - 04	8.26e - 04
3	$1.00e{-01}$	1.37 <i>e</i> +00	6	1.00e - 01	1.37e+00
3	1.00e - 02	$8.21e{-02}$	6	1.00e - 02	9.00e - 02
3	1.00e - 03	3.21e-02	6	1.00e - 03	9.69e - 04
3	1.00e - 04	3.22e-02	6	1.00e - 04	1.15e - 04
4	1.00e - 01	1.37 <i>e</i> +00	7	1.00e - 01	1.37e+00
4	1.00e - 02	8.77e - 02	7	1.00e - 02	9.00e - 02
4	1.00e - 03	5.54e - 03	7	1.00e - 03	9.63e - 04
4	1.00e - 04	5.47e - 03	7	1.00e - 04	9.64e - 06

Table 1 Burgers equation, ROM differential filter, smooth initial condition, $\nu = 10^{-1}$, and d = 7: Average CE for different δ and r values

where $\overline{}^r$ represents the ROM projection filter. We denote with a_r, a_d, b_r and c_r the coefficient vectors of the basis functions in $\overline{u_d}^r$, u_d , $\Delta \overline{u_d}^r$, and $\overline{\Delta u_d}^r$, respectively. We start by evaluating $\Delta \overline{u_d}^r$:

$$(\Delta \overline{u_d}^r, \phi_i) = -(\nabla \overline{u_d}^r, \nabla \phi_i), \quad \forall i = 1, ..., r.$$
(30)

Its corresponding linear system is

$$M_r \, \boldsymbol{b}_r = -S_r \, \boldsymbol{a}_r. \tag{31}$$

Using (13) and (31), we have

$$\boldsymbol{b}_r = -M_r^{-1} S_r M_r^{-1} M_{r \times d} \, \boldsymbol{a}_d. \tag{32}$$

Next, we evaluate $\overline{\Delta u_d}^r$. By using (12) for $\overline{\Delta u_d}^r$, we have:

$$(\overline{\Delta u_d}^r, \phi_i) = (\Delta u_d, \phi_i) = -(\nabla u_d, \nabla \phi_i), \quad \forall i = 1, ..., r,$$
(33)

which yields

$$\boldsymbol{c}_r = -M_r^{-1} S_{r \times d} \, \boldsymbol{a}_d. \tag{34}$$

Again, we note that the right hand sides of the equations (32) and (34) are not equal. This suggests that, in some cases, for the ROM projection filter, the Laplacian CE can be nonzero:

$$\mathcal{E}_{\Delta}[\boldsymbol{u}_d] = \sum_{i=1}^r (\boldsymbol{b}_r - \boldsymbol{c}_r)_j \, \boldsymbol{\phi}_j \neq 0. \tag{35}$$

In the tests used in the numerical investigation in Section 5, the Laplacian CE is nonzero (see, e.g., Tables 2, 6, 10, 14, 18, and 21).

Again, we note that the vectors $\mathbf{b_r}$ in (32) and $\mathbf{c_r}$ in (34), which are needed in the calculation of the Laplacian CE in (35), involve only the ROM mass matrices M_r and



Table 2 Burgers equation, ROM projection filter, smooth initial condition, $\nu = 10^{-1}$, and d = 7: Average CE and average ROM subfilter-scale stress tensor for different r values

r	$ \mathcal{E}_{\Delta}[u_d] _{L^2(L^2)}$	$ \tau _{L^2(L^2)}$
2	1.54e - 01	6.51e - 03
3	3.22e - 02	1.01e - 03
4	5.47e - 03	1.35e - 04
5	8.26e - 04	1.69e - 05
6	1.15e - 04	1.96e - 06
7	0	0

 $M_{r \times d}$ and the ROM stiffness matrices S_r and $S_{r \times d}$, which can be computed with low order finite element discretizations, such as those that we use in Section 5.

4 Effect of commutation error on DDC-ROM

In this section, we investigate the effect of the commutation error on three LES-ROMs that are built from equations (18)–(20) supplemented with the Laplacian CE (9). The first LES-ROM that we investigate is the data-driven correction ROM (DDC-ROM) [44], which utilizes available data to construct an r-dimensional model for the Correction term (i.e., the ROM subfilter-scale stress tensor) τ in (18)–(20); the DDC-ROM, however, does not include a model for the Laplacian CE (9). The second LES-ROM that we consider is the ideal CE data-driven correction ROM (ICE-DDC-ROM), which is the DDC-ROM supplemented with an exact (fine) resolution Laplacian CE (9). The third LES-ROM that we investigate is the commutation error DDC-ROM (CE-DDC-ROM), which is the DDC-ROM supplemented with an r-dimensional data-driven model for the Laplacian CE (9). In Section 5, we investigate numerically whether the Laplacian CE has any effect on the DDC-ROM, i.e., whether the ICE-DDC-ROM and the CE-DDC-ROM yield more accurate results than the standard DDC-ROM. In this section, we outline the construction of the DDC-ROM, ICE-DDC-ROM, and CE-DDC-ROM.

First, we briefly derive the standard Galerkin-ROM (G-ROM). The ROM approximation of the velocity is defined as

$$\boldsymbol{u}_r(\mathbf{x},t) = \sum_{i=1}^r (\boldsymbol{a}_r)_j(t) \boldsymbol{\phi}_j(\mathbf{x}), \tag{36}$$

where $\{(a_r)_j\}_{j=1}^r(t)$ are the sought time-dependent coefficients, which are found by solving the following system of PDEs: $\forall i = 1, ..., r$,

$$\left(\frac{\partial \boldsymbol{u}_r}{\partial t}, \boldsymbol{\phi}_i\right) + \nu(\nabla \boldsymbol{u}_r, \nabla \boldsymbol{\phi}_i) + ((\boldsymbol{u}_r \cdot \nabla)\boldsymbol{u}_r, \boldsymbol{\phi}_i) = 0, \tag{37}$$

where we assume that the modes $\{\phi_1, \phi_2, \cdots, \phi_r\}$ are perpendicular to the discrete pressure space. This assumption holds if in the snapshot creation we use mixed FE



such as Scott-Vogelius, or the mini-element; see, e.g., [6, 20]. Plugging (36) into (37) gives the *Galerkin ROM (G-ROM)*:

$$\dot{a_r} = Aa_r + a_r^{\top} Ba_r, \tag{38}$$

which can be written componentwise as follows: $\forall i = 1, ... r$,

$$\dot{a}_i = \sum_{m=1}^r A_{im} \, a_m(t) + \sum_{m=1}^r \sum_{n=1}^r B_{imn} \, a_n(t) \, a_m(t) \,, \tag{39}$$

where $A_{im} = -\nu(\nabla \phi_m, \nabla \phi_i)$ and $B_{imn} = -(\phi_m \cdot \nabla \phi_n, \phi_i), 1 \le i, m, n \le r$.

To construct the DDC-ROM, ICE-DDC-ROM, and CE-DDC-ROM, we utilize the same approach as that used in Section 3.2 to derive LES-ROMs. However, we emphasize that in contrast to Section 3.2, this time we do *not* assume that spatial filtering and differentiation commute. Instead, we model the Laplacian CE (9) in two of the LES-ROMs (i.e., ICE-DDC-ROM and CE-DDC-ROM). Next, we summarize the construction of the three LES-ROMs: (i) in the F-NSE (7), we replace \boldsymbol{u} with \boldsymbol{u}_d (as we did in Section 3.2); (ii) in the Laplacian term, we interchange filtering and differentiation, and then we add the resulting Laplacian CE (9); and (iii) we replace the filtered nonlinear term with the nonlinear term of the filtered variables (i.e., $((\boldsymbol{u}_r \cdot \nabla)\boldsymbol{u}_r, \boldsymbol{\phi}_i))$) and then we add the resulting ROM subfilter-scale stress tensor $\boldsymbol{\tau}_r^{SFS}$ defined in (20). This construction yields the following ROM: $\forall i=1,\cdots,r$,

$$\left(\frac{\partial \boldsymbol{u}_r}{\partial t}, \boldsymbol{\phi}_i\right) + \nu(\nabla \boldsymbol{u}_r, \nabla \boldsymbol{\phi}_i) + ((\boldsymbol{u}_r \cdot \nabla)\boldsymbol{u}_r, \boldsymbol{\phi}_i)
+ \nu(\mathcal{E}_{\Delta}[\boldsymbol{u}_d], \boldsymbol{\phi}_i) + (\boldsymbol{\tau}_r^{SFS}, \boldsymbol{\phi}_i) = 0.$$
(40)

Equation (40) yields the following dynamical system:

$$\dot{\boldsymbol{a}}_r = A\boldsymbol{a}_r + \boldsymbol{a}_r^{\top}B\boldsymbol{a}_r + \mathcal{E}_{CE} + \boldsymbol{\tau}, \tag{41}$$

where A and B are the same as in (38) and the components of \mathcal{E}_{CE} and τ are given by: $\forall i = 1, ..., r$,

$$(\mathcal{E}_{CE})_i = -\nu(\mathcal{E}_{\Delta}[\boldsymbol{u}_d], \boldsymbol{\phi}_i), \tag{42}$$

$$\tau_i = -(\tau_r^{SFS}, \phi_i). \tag{43}$$

To construct the DDC-ROM [44], we make the following ansatz:

$$\tau \approx \tau^{\text{ansatz}}(\boldsymbol{a}_r) = \tilde{A}\boldsymbol{a}_r + \boldsymbol{a}_r^{\top} \tilde{B}\boldsymbol{a}_r.$$
 (44)

As mentioned in [44], we choose the quadratic ansatz (44) to resemble the right hand side of the G-ROM (38). We note, however, that other ansatz forms can be considered; we plan to investigate those in a future study.

To compute the operators A and B in (44), we use data-driven modeling ensuring the highest accuracy of the vector τ . To this end, we solve the following unconstrained optimization problem:

$$\min_{\tilde{A} \in \mathbb{R}^{r \times r}} \sum_{j=1}^{M} \| \boldsymbol{\tau}(t_j) - \boldsymbol{\tau}^{\text{ansatz}}(\boldsymbol{a}_r(t_j)) \|^2.$$

$$\tilde{B} \in \mathbb{R}^{r \times r \times r}} \sum_{j=1}^{M} \| \boldsymbol{\tau}(t_j) - \boldsymbol{\tau}^{\text{ansatz}}(\boldsymbol{a}_r(t_j)) \|^2.$$
(45)



The data-driven correction ROM (DDC-ROM) has the following form:

$$\dot{\mathbf{a}}_r = (A + \tilde{A})\mathbf{a}_r + \mathbf{a}_r^{\top}(B + \tilde{B})\mathbf{a}_r, \tag{46}$$

where the operators A and B are the G-ROM operators in (38) and the operators \tilde{A} and \tilde{B} are the solution of the unconstrained minimization problem (45).

Remark 2 (DDC-ROM) The DDC-ROM was proposed in [44] and further improved in [25]. Details regarding the DDC-ROM construction, including the numerical solution of the ill-conditioned linear least squares problem corresponding to (45) by using the truncated singular value decomposition, are presented in Algorithm 1 in [44]. The computational efficiency of the DDC-ROM is discussed in Section 5.3 in [44]. Finally, a physically constrained DDC-ROM, which aims at improving the physical accuracy of the DDC-ROM, is proposed in [25]. The physical constraints require that the DDC-ROM operators satisfy the same type of physical laws as those satisfied by the NSE and replace (45) with a constrained least squares problem. The numerical results in [25] show that the physically constrained DDC-ROM is significantly more stable and accurate than the standard DDC-ROM. However, since the main focus of this paper is the investigation of ROM spatial filtering and the corresponding CE, we only consider the standard DDC-ROM.

The *ideal commutation error DDC-ROM (ICE-DDC-ROM)* is obtained by adding a high-accuracy (i.e., from fine resolution numerical data) representation of the Laplacian CE (9):

$$\dot{\boldsymbol{a}}_r = (A + \tilde{A})\boldsymbol{a}_r + \boldsymbol{a}_r^{\top}(B + \tilde{B})\boldsymbol{a}_r + \mathcal{E}_{CE}. \tag{47}$$

To construct the CE-DDC-ROM, we make the following ansatz:

$$(\tau + \mathcal{E}_{CE}) \approx (\tau + \mathcal{E}_{CE})^{\text{ansatz}}(\boldsymbol{a}_r) = \tilde{A}\boldsymbol{a}_r + \boldsymbol{a}_r^{\top} \tilde{B}\boldsymbol{a}_r.$$
 (48)

To compute the operators \tilde{A} and \tilde{B} in (47), we use data-driven modeling ensuring the highest accuracy of the vector $\tau + \mathcal{E}_{CE}$. To this end, we solve the following unconstrained optimization problem:

$$\min_{\tilde{A} \in \mathbb{R}^{r \times r}} \sum_{j=1}^{M} \| (\tau + \mathcal{E}_{CE})(t_j) - (\tau + \mathcal{E}_{CE})^{\text{ansatz}} (\boldsymbol{a}_r(t_j)) \|^2.$$
 (49)

The commutation error data-driven ROM (CE-DDC-ROM) has the following form:

$$\dot{\mathbf{a}}_r = (A + \tilde{A})\mathbf{a}_r + \mathbf{a}_r^{\top}(B + \tilde{B})\mathbf{a}_r, \tag{50}$$

where the operators A and B are the G-ROM operators in (38) and the operators \tilde{A} and \tilde{B} are the solution of the unconstrained minimization problem (49).

5 Numerical experiments

In this section, we investigate numerically the following questions:



- (Q1) How large is the CE?
- (Q2) Does the CE have a significant effect on ROMs? Should the commutation error be modeled?

To answer the first question, we evaluate numerically the Laplacian CE and compute its average, i.e., $||\mathcal{E}_{\Delta}[\mathbf{u}_d]||_{L^2(L^2)}$, which is calculated as follows:

$$\sqrt{\frac{\int_0^T \|\mathcal{E}_{\Delta}[\boldsymbol{u}_d]\|^2 dt}{T}} \approx \sqrt{\frac{\Delta t \sum_{j=1}^M (\mathbf{b}_r(t_j) - \mathbf{c}_r(t_j))^\top M_r(\mathbf{b}_r(t_j) - \mathbf{c}_r(t_j))}{T}}.$$

Furthermore, we also compare the average of the Laplacian CE with the average of the ROM subfilter-scale tensor, which we used in Section 4 to construct the DDC-ROM (46), the ICE-DDC-ROM (47), and the CE-DDC-ROM (50). We calculate the average of the ROM subfilter-scale tensor, $||\tau||_{L^2(L^2)}$, as follows:

$$\sqrt{\frac{\int_0^T \|\tau\|^2 dt}{T}} \approx \sqrt{\frac{\Delta t \sum_{j=1}^M \tau(t_j)^\top M_r \, \tau(t_j)}{T}},$$

where the vector τ is defined in (15).

To answer the second question, we test the following ROMs: the DDC-ROM (46), the ICE-DDC-ROM (47), and the CE-DDC-ROM (50). We emphasize that the ICE-DDC-ROM and CE-DDC-ROM include a representation of the Laplacian CE (9), whereas the DDC-ROM does not. Thus, if the ICE-DDC-ROM and CE-DDC-ROM yield more accurate results than the DDC-ROM, we conclude that the CE plays a significant role in ROM development. In our numerical investigation, we consider two test problems: the 1D viscous Burgers equation (Section 5.1) and the 2D channel flow past a circular cylinder (Section 5.2).

To compute the norm of the error in the numerical experiments, we use the following formula:

$$\left\| \boldsymbol{u}_r - \sum_{i=1}^r \left(\boldsymbol{u}^{DNS}, \boldsymbol{\phi}_i \right) \boldsymbol{\phi}_i \right\| , \tag{51}$$

where u_r is the ROM approximation and u^{DNS} is the direct numerical simulation (DNS) solution. Thus, we compute the ROM error as the difference between the ROM approximation and the DNS solution projected onto the ROM space, X^r . We emphasize that, while the metric (51) has been utilized in other studies [25, 44], alternative metrics could be used instead (see, e.g., [17] and the discussion in Section 5.4).

5.1 Experiment 1: Burgers equation

In our first experiment, we consider the Burgers equation:

$$\begin{cases} u_t - vu_{xx} + uu_x = 0, & x \in [0, 1], \ t \in [0, 1] \\ u(0, t) = u(1, t) = 0, & t \in [0, 1]. \end{cases}$$
 (52)

The DNS results are obtained by using a linear FE scheme with mesh width h = 1/2048 and timestep size $\Delta t = 10^{-3}$.



In this section, we compute d (i.e., the rank of the snapshot matrix Y) as the number of singular values of the matrix $\frac{1}{M}YY^TM_h$ that are larger than the prescribed tolerance 1.0e-15.

To investigate the effect of initial conditions, we consider a smooth initial condition (Section 5.1.1) and a non-smooth initial condition (Section 5.1.2). Furthermore, to investigate the effect of the viscosity parameter, we consider two viscosity values: $\nu = 10^{-1}$ (Sections 5.1.1 and 5.1.2) and $\nu = 10^{-3}$ (Section 5.1.3).

5.1.1 Smooth initial condition

We consider the initial condition

$$u_0(x) = \frac{2\nu\beta\pi \, \sin(\pi x)}{\alpha + \beta \, \cos(\pi x)} \,, \quad x \in [0, 1], \tag{53}$$

where $\alpha = 5$ and $\beta = 4$.

First, we address (Q1), i.e., we investigate the size of the CE. For various r and δ values, we list the CE computed by using the ROM differential filter (Table 1) and the ROM projection filter (Table 2). The main conclusion is that the CE exists for both filters, especially for low r values. We also observe that as r increases, the CE decreases. Finally, we note that, for the ROM differential filter (Table 1), for a fixed r value, as δ decreases, the CE decreases.

In Table 2, in addition to the CE average, we also list the ROM subfilter-scale stress tensor average for different *r* values. We observe that the CE average is larger than the ROM subfilter-scale stress tensor average.

Next, we address (Q2), i.e., we investigate whether the CE has a significant effect on ROMs. To this end, we test the DDC-ROM (46), the ICE-DDC-ROM (47), and the CE-DDC-ROM (50). We note that the ICE-DDC-ROM and CE-DDC-ROM include a representation of the Laplacian CE (9), whereas the DDC-ROM does not. For various r and δ values, we list the ROM error, computed by using the metric (51), the ROM differential filter (Table 3), and the ROM projection filter (Table 4). The δ values used in Table 3 are computed by trial and error: for a given ROM and r value, we select the δ value that yields the most accurate results.

In Fig. 1, we plot the sensitivity of the CE-DDC-ROM error with respect to δ . We notice that the smallest error is attained for small values of δ . This could be related to the use of the L^2 error metric norm in this paper; other norms (e.g., the H^1 norm) could yield different conclusions.

The errors in Tables 3 and 4 are computed by using formula (51). We observe that the ICE-DDC-ROM and CE-DDC-ROM errors are consistently lower than the DDC-ROM error. We emphasize that, for low r values, the ICE-DDC-ROM and CE-DDC-ROM errors are *two and even three orders of magnitude* lower than the DDC-ROM error. Thus, we conclude that the CE plays a significant role in ROM development. Tables 3 and 4 also show that, as r increases, the DDC-ROM error approaches the ICE-DDC-ROM and CE-DDC-ROM errors. We also note that the δ values in Table 3 are small. Thus, in this case, the effect of the ROM differential filter is similar to the effect of the ROM projection filter.



Table 3	Burgers equation, ROM differential filter, smooth initial condition, $v = 10^{-1}$, and $d = 7$: Average
error in	G-ROM, DDC-ROM, ICE-DDC-ROM, and CE-DDC-ROM for different δ and r values

r	δ	G-ROM	δ	DDC-ROM
2	-	1.78 <i>e</i> -03	1.00 <i>e</i> -05	1.32 <i>e</i> -03
3	_	1.93e - 04	1.00e - 05	1.55e - 04
4	_	2.00e-05	1.00e - 04	1.69e - 05
5	_	2.03e-06	1.00e - 04	1.77e - 06
6	_	2.23e-07	1.00e - 05	2.02e-07
7	_	9.56e - 08	1.00e-05	9.55e - 08
r	δ	ICE-DDC-ROM	δ	CE-DDC-ROM
2	1.00 <i>e</i> -04	1.46e - 05	1.00e - 04	$1.48e{-05}$
3	1.00 <i>e</i> -06	1.73e - 07	1.00e - 06	1.55e - 07
4	1.00 <i>e</i> -06	9.46e - 08	1.00e - 06	9.49e - 08
5	1.00e-05	9.23e - 08	1.00e - 05	9.25e - 08
6	1.00e-05	9.37e - 08	1.00e - 05	$9.38e{-08}$
7	1.00 <i>e</i> -08	9.56e - 08	1.00e-05	9.56e - 08

Table 4 Burgers equation, ROM projection filter, smooth initial condition, $v = 10^{-1}$, and d = 7: Average error in G-ROM, DDC-ROM, ICE-DDC-ROM, and CE-DDC-ROM for different r values

r	G-ROM	DDC-ROM	ICE-DDC-ROM	CE-DDC-ROM
2	1.78 <i>e</i> -03	1.32 <i>e</i> -03	1.46e-05	1.48 <i>e</i> -05
3	1.93e - 04	1.55e - 04	1.73e - 07	1.55e - 07
4	2.00e-05	7.40e - 06	8.72e - 08	$8.90e{-08}$
5	2.03e - 06	7.29e - 07	9.23e - 08	$9.25e{-08}$
6	2.23e-07	1.60e - 07	9.35e - 08	$9.35e{-08}$
7	9.56e - 08	9.56e - 08	9.56e - 08	9.56e - 08

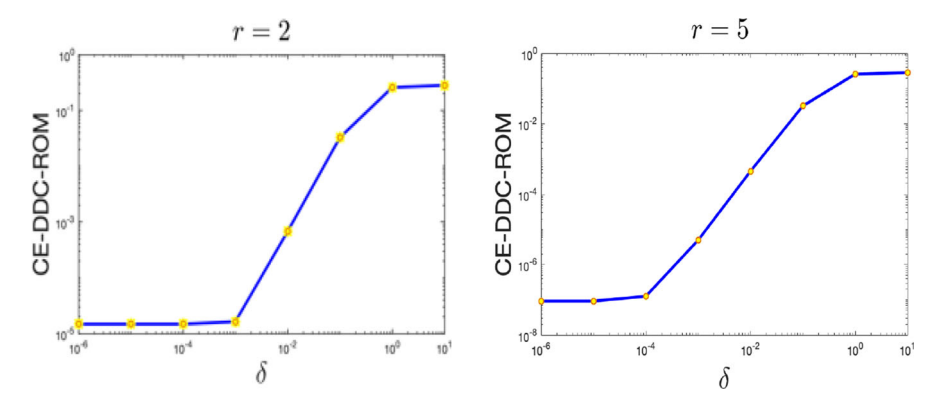


Fig. 1 Burgers equation, ROM differential filter, smooth initial condition, $v=10^{-1}$, r=2, 5: Sensitivity plots of the CE-DDC-ROM error with respect to δ



5.1.2 Non-smooth initial condition

In this section, we investigate the effect of non-smooth initial conditions on the results obtained in Section 5.1.1. To this end, we consider the following initial condition:

$$u_0(x) = \begin{cases} 1, & x \in (0, 1/2], \\ 0, & x \in (1/2, 1]. \end{cases}$$
 (54)

As initial conditions in the FE and ROM discretizations, we use the L^2 projection of (54) on the FE and ROM spaces, respectively.

As in Section 5.1.1, we start by addressing (Q1), i.e., we measure the size of the CE. For various r and δ values, we list the CE computed by using the ROM differential filter (Table 5) and the ROM projection filter (Table 6). We draw the same main conclusion as in Section 5.1.1: The CE exists for both filters.

This time, however, as r increases, the CE increases. Furthermore, for the ROM differential filter (Table 5), we note that for low r values, as δ decreases, the CE increases.

In Table 6, in addition to the CE average, we also list the ROM subfilter-scale stress tensor average for different r values. The CE average is significantly larger than the ROM subfilter-scale stress tensor average.

Table 5 Burgers equation, ROM differential filter, non-smooth initial condition, $\nu = 10^{-1}$, and d = 19: Average CE for different δ and r values

r	δ	$ \mathcal{E}_{\Delta}[u_d] _{L^2(L^2)}$	r	δ	$ \mathcal{E}_{\Delta}[u_d] _{L^2(L^2)}$
2	1.00e-01	1.85 <i>e</i> +00	9	1.00e-01	2.13 <i>e</i> +00
2	1.00e - 02	1.12 <i>e</i> +00	9	1.00e - 02	2.25e+01
2	1.00e - 03	1.90e+00	9	1.00e - 03	7.12 <i>e</i> +02
2	1.00e - 04	4.18 <i>e</i> +00	9	1.00e - 04	1.27 <i>e</i> +02
2	1.00e - 05	4.29e+00	9	1.00e - 05	1.17e+02
3	$1.00e{-01}$	2.71e+00	11	1.00e - 01	2.13e+00
3	1.00e-02	6.70e+00	11	1.00e - 02	2.14e+01
3	1.00e - 03	1.07 <i>e</i> +01	11	1.00e - 03	7.14 <i>e</i> +02
3	1.00e-04	2.68e+01	11	1.00e - 04	8.15 <i>e</i> +01
3	1.00e - 05	2.75 <i>e</i> +01	11	1.00e - 05	3.59e+01
5	$1.00e{-01}$	2.13 <i>e</i> +00	17	1.00e - 01	2.13 <i>e</i> +00
5	1.00e-02	5.00e+01	17	1.00e - 02	2.13e+01
5	1.00e - 03	2.35e+02	17	1.00e - 03	6.36e+02
5	1.00e - 04	3.15 <i>e</i> +02	17	1.00e - 04	1.10e+02
5	1.00e - 05	3.25 <i>e</i> +02	17	1.00e - 05	1.29e+00
7	1.00e - 01	2.11 <i>e</i> +00	19	$1.00e{-01}$	2.13 <i>e</i> +00
7	1.00e - 02	2.90e+01	19	1.00e-02	2.13e+01
7	1.00e - 03	6.25 <i>e</i> +02	19	1.00e - 03	6.05e+02
7	1.00e - 04	2.95 <i>e</i> +02	19	1.00e - 04	1.20e+02
7	1.00e - 05	3.04 <i>e</i> +02	19	1.00e - 05	1.29e+00



Table 6 Burgers equation, ROM projection filter, non-smooth initial condition, $v = 10^{-1}$, and d = 19: Average CE and average ROM subfilter-scale stress tensor for different r values

r	$ \mathcal{E}_{\Delta}[u_d] _{L^2(L^2)}$	$ \tau _{L^2(L^2)}$
2	4.29e + 00	5.68e - 02
3	2.75e + 01	3.69e - 02
5	3.25e + 02	2.73e - 02
7	3.04e + 02	1.05e - 02
9	1.17e + 02	3.46e - 03
11	3.60e + 01	9.99e - 04
17	5.27e - 01	1.39e - 05

Next, we address (Q2), i.e., we investigate whether the CE has a significant effect on ROMs. As in Section 5.1.1, we test the DDC-ROM (46), the ICE-DDC-ROM (47), and the CE-DDC-ROM (50). We note again that the ICE-DDC-ROM and CE-DDC-ROM include a representation of the Laplacian CE (9), whereas the DDC-ROM does not. For various r and δ values, we list the ROM error, computed by using the metric (51), the ROM differential filter (Table 7), and the ROM projection filter (Table 8). We draw the same main conclusion as in Section 5.1.1: The ICE-DDC-ROM and CE-DDC-ROM errors are consistently lower than the DDC-ROM errors

Table 7 Burgers equation, ROM differential filter, non-smooth initial condition, $\nu = 10^{-1}$, and d = 19: Average error in G-ROM, DDC-ROM, ICE-DDC-ROM, and CE-DDC-ROM for different δ and r values

r	δ	G-ROM	δ	DDC-ROM
2	_	7.27 <i>e</i> -03	1.00e-05	6.93 <i>e</i> -03
3	_	1.51e - 02	1.00e - 04	$8.16e{-03}$
5	_	4.22e - 03	1.00e - 04	4.22e-03
7	_	9.59e - 04	1.00e - 04	9.59e - 04
9	_	2.34e - 04	1.00e - 04	2.35e - 04
11	_	5.44e - 05	1.00e - 07	5.56e - 05
17	_	4.97e - 07	1.00e - 07	5.06e - 07
19	_	1.30e - 07	1.00e-07	1.30e - 07
r	δ	ICE-DDC-ROM	δ	CE-DDC-ROM
2	1.00e - 03	2.67e - 04	1.00e - 02	1.07e - 03
3	1.00e - 04	5.85e - 05	1.00e - 02	1.36e - 03
5	1.00e - 07	5.97e - 07	1.00e - 04	3.13e-04
7	1.00e - 07	1.32e - 07	1.00e - 04	6.27e - 05
9	1.00e - 06	1.42e - 07	1.00e - 05	2.07e - 06
11	1.00e - 07	1.38e - 07	1.00e-06	1.48e - 07
17	1.00e - 07	1.35e - 07	1.00e - 07	1.19e - 07
19	1.00e-07	1.30e-07	1.00e-07	1.30e - 07



G-ROM DDC-ROM ICE-DDC-ROM CE-DDC-ROM r 2 7.27e - 036.93e - 032.71e - 043.71e - 033 1.51e - 028.14e - 033.84e - 035.89e - 055 4.22e - 034.22e - 035.97e - 073.14e - 047 9.59e - 049.59e - 046.44e - 051.32e - 079 2.34e - 042.34e - 041.39e - 074.26e - 065.44e - 055.44e - 051.30e - 071.28e - 0711 17 4.97e - 075.00e - 071.34e - 071.15e - 0719 1.30e - 071.30e - 071.30e - 071.30e - 07

Table 8 Burgers equation, ROM projection filter, non-smooth initial condition, $v = 10^{-1}$, and d = 19: Average error in G-ROM, DDC-ROM, ICE-DDC-ROM, and CE-DDC-ROM for different r values

and the G-ROM errors. Furthermore, for low r values, the ICE-DDC-ROM and CE-DDC-ROM errors are *one and even two orders of magnitude* lower than the DDC-ROM error. Thus, we conclude again that the CE plays a significant role in ROM development. Tables 7 and 8 also show that, as r increases, the DDC-ROM error approaches the ICE-DDC-ROM and CE-DDC-ROM errors.

5.1.3 Lower viscosity ($v = 10^{-3}$)

In this section, we investigate the effect of lower viscosity on the results obtained in Sections 5.1.1 and 5.1.2. The low viscosity results for the smooth initial condition used in Section 5.1.1 are similar to the low viscosity results for the non-smooth initial condition used in Section 5.1.2. Thus, for clarity, we only present the former. As in the previous sections, we start by addressing (Q1), i.e., we measure the size of the CE. For various r and δ values, we list the CE computed by using the ROM differential filter (Table 9) and the ROM projection filter (Table 10). We draw the same main conclusion as in Sections 5.1.1 and 5.1.2: The CE exists for both filters.

In Table 10, in addition to the CE average, we also list the ROM subfilter-scale stress tensor average for different r values. As in Sections 5.1.1 and 5.1.2, the CE average is larger than the ROM subfilter-scale stress tensor average.

Next, we address (Q2), i.e., we investigate whether the CE has a significant effect on ROMs. As in Sections 5.1.1 and 5.1.2, we test the DDC-ROM (46), the ICE-DDC-ROM (47), and the CE-DDC-ROM (50). We note again that the ICE-DDC-ROM and CE-DDC-ROM include a representation of the Laplacian CE (9), whereas the DDC-ROM does not. For various r and δ values, we list the ROM error, computed by using the metric (51), the ROM differential filter (Table 11), and the ROM projection filter (Table 12). We draw the same main conclusion as in Sections 5.1.1 and 5.1.2: The ICE-DDC-ROM and CE-DDC-ROM errors are consistently lower than the DDC-ROM errors and the G-ROM errors. Furthermore, for low r values, the ICE-DDC-ROM and CE-DDC-ROM errors are two and even three orders of magnitude lower than the DDC-ROM error. Thus, we conclude again that the CE plays a significant



Table 9 Burgers equation, ROM differential filter, smooth initial condition, $\nu = 10^{-3}$, and d = 3: Average CE for different δ and r values

r	δ	$ \mathcal{E}_{\Delta}[u_d] _{L^2(L^2)}$
1	$1.00e{-01}$	3.61e - 04
1	$1.00e{-02}$	4.39e - 04
1	$1.00e{-04}$	4.40e - 04
1	$1.00e{-06}$	4.40e - 04
2	$1.00e{-01}$	2.09e-06
2	$1.00e{-02}$	4.28e - 06
2	$1.00e{-04}$	4.32e - 06
2	$1.00e{-06}$	4.32e - 06
3	$1.00e{-01}$	$1.36e{-15}$
3	1.00e - 02	4.80e - 17
3	$1.00e{-04}$	3.80e - 17
3	1.00e-06	3.74e - 17

role in ROM development. We also note that, for the Burgers equation, the lower viscosity ($\nu = 10^{-3}$) results are similar to the higher viscosity ($\nu = 10^{-1}$) results.

5.2 Experiment 2: flow past a circular cylinder

In our second experiment, we consider a 2D channel flow past a circular cylinder. The domain is a 2.2×0.41 rectangular channel with a radius = 0.05 cylinder, centered at (0.2, 0.2), see Fig. 2. No slip boundary conditions are prescribed on the walls and cylinder, and the inflow and outflow profiles are given by [25, 26]

$$u_1(0, y, t) = u_1(2.2, y, t) = \frac{6}{0.41^2}y(0.41 - y),$$

 $u_2(0, y, t) = u_2(2.2, y, t) = 0,$

where $\boldsymbol{u} = \langle u_1, u_2 \rangle$.

Although imposing a parabolic profile for the outflow velocity is unphysical, we note that the Dirichlet boundary conditions are common in the ROM field, since they simplify the theoretical and numerical investigation. We also emphasize that these outflow velocity boundary conditions do not significantly affect the upstream drag and lift coefficients [19, 35].

There is no forcing (f = 0) and the flow starts from rest. We run the DNS of the NSE (4)–(5) from rest (t = 0) until the final simulation time T = 17. We use

Table 10 Burgers equation, ROM projection filter, smooth initial condition, $v = 10^{-3}$, and d = 3: Average CE and average ROM subfilter-scale stress tensor for different r values

r	$ \mathcal{E}_{\Delta}[u_d] _{L^2(L^2)}$	$ \tau _{L^2(L^2)}$
1	4.40e - 04	2.71e - 07
2	4.32e - 06	1.73e - 09
3	0	0
-		-



Table 11 Burgers equation, ROM differential filter, smooth initial condition, $v = 10^{-3}$, and d = 3: Average error in G-ROM, DDC-ROM, ICE-DDC-ROM, and CE-DDC-ROM for different δ and r values

r	δ	G-ROM	δ	DDC-ROM
1	_	2.21e-07	1.00e-03	5.81 <i>e</i> -08
2	_	$9.33e{-10}$	1.00e - 08	$6.68e{-10}$
3	_	3.46e - 12	1.00e - 08	$3.46e{-12}$
r	δ	ICE-DDC-ROM	δ	CE-DDC-ROM
1	1.00 <i>e</i> -05	$3.50e{-10}$	1.00e-06	4.07e - 10
2	1.00 <i>e</i> -08	5.35e - 13	1.00e - 08	5.37 <i>e</i> -13
3	1.00 <i>e</i> -08	3.46e - 12	1.00e-08	$3.46e{-12}$

the point-wise divergence-free, LBB stable (P_2, P_1^{disc}) Scott-Vogelius FE pair on a barycenter refined regular triangular mesh [20]. The mesh provides 35K velocity degrees of freedom for Re=100 case, and 103K velocity degrees of freedom for Re=500 case. The time step size $\Delta t=0.002$ is used for both DNS and ROM time evolution. We utilize the commonly used linearized BDF2 temporal discretization, together with the FE spatial discretization. On the first time step, we use a backward Euler scheme so that we have two initial time step solutions required for the BDF2 scheme. The scheme for $n=1,2,\cdots$, is: Find $(\boldsymbol{u}_h^{n+1},p_h^{n+1})\in(X^h,Q^h)$ satisfying for every $(\boldsymbol{v}_h,q_h)\in(X^h,Q^h)$,

$$\left(\frac{3\boldsymbol{u}_{h}^{n+1} - 4\boldsymbol{u}_{h}^{n} + \boldsymbol{u}_{h}^{n-1}}{2\Delta t}, \boldsymbol{v}_{h}\right) + \left(\left(2\boldsymbol{u}_{h}^{n} - \boldsymbol{u}_{h}^{n-1}\right) \cdot \nabla \boldsymbol{u}_{h}^{n+1}, \boldsymbol{v}_{h}\right) - \left(p_{h}^{n+1}, \nabla \cdot \boldsymbol{v}_{h}\right) + \nu\left(\nabla \boldsymbol{u}_{h}^{n+1}, \nabla \boldsymbol{v}_{h}\right) = 0,$$

$$(\nabla \cdot \boldsymbol{u}_{h}, q_{h}) = 0.$$
(55)

In this section, we compute d (i.e., the rank of the snapshot matrix Y) as the number of singular values of the matrix $\frac{1}{M}YY^TM_h$ that are larger than the prescribed tolerance 1.0e-05.

Table 12 Burgers equation, ROM projection filter, smooth initial condition, $\nu = 10^{-3}$, and d = 3: Average error in G-ROM, DDC-ROM, ICE-DDC-ROM, and CE-DDC-ROM for different r values

r	G-ROM	DDC-ROM	ICE-DDC-ROM	CE-DDC-ROM
1	2.21e-07	1.35e - 07	3.49e - 10	4.07e - 10
2	$9.33e{-10}$	$6.68e{-10}$	5.35e - 13	5.37e - 13
3	3.46e - 12	$3.46e{-12}$	3.46e - 12	$3.46e{-12}$





Fig. 2 Geometry of the flow past a circular cylinder numerical experiment

5.2.1 Reynolds number Re = 100

In this section, we present numerical results for Re = 100, where the Reynolds number is calculated with $v = 10^{-3}$ and the diameter of the cylinder as the characteristic length scale. To generate the ROM basis, we collect 1501 snapshots, which are the FE solutions at each time step from t = 7 to t = 10. The time interval [7, 10] does not include the initial transient. We take the FE solution at t = 7 as the initial ROM solution. To construct the ROM subfilter-scale stress tensor and the CE in the DDC-ROM (46), the ICE-DDC-ROM (47), and the CE-DDC-ROM (50), we use 166 snapshots, which are the FE solutions at each time step from t = 7.002 to t = 7.332. We note that the time interval [7.002, 7.332] represents one period; using snapshots from more than one period to construct the ROM subfilter-scale stress tensor and the CE does not improve the accuracy of the results.

As in Section 5.1, we address questions (Q1) and (Q2). We start with (Q1), i.e., we measure the size of the CE. For various r and δ values, we list the CE computed by using the ROM differential filter (Table 13) and the ROM projection filter (Table 14). The main conclusion is that the CE exists for both filters, just as for the Burgers equation in Section 5.1.

Table 12	NICE D.	100 DOM	1:cc	1 14. 4	OF 6 1:66	
Table 13	NSE. $Ke =$	= 100. KOW	differential filter.	a = 14: Average	e CE for differer	It δ and r values

r	$\delta = 1.00e - 04$	$\delta = 1.00e - 03$	$\delta = 1.00e - 2$	$\delta = 1.00e - 01$	$\delta = 1.50e - 01$
2	1.05e+01	1.05 <i>e</i> +01	1.02e+01	3.42 <i>e</i> +00	1.90e+00
3	1.01 <i>e</i> +01	1.01 <i>e</i> +01	9.48 <i>e</i> +00	1.71 <i>e</i> +00	$8.98e{-01}$
4	1.85 <i>e</i> +01	1.84 <i>e</i> +01	1.53 <i>e</i> +01	1.13 <i>e</i> +00	5.33e - 01
5	2.39e+01	2.38e+01	1.95e+01	1.18 <i>e</i> +00	5.45e - 01
6	2.50e+01	2.49 <i>e</i> +01	1.98 <i>e</i> +01	1.01 <i>e</i> +00	4.63e - 01
7	3.03 <i>e</i> +01	3.03 <i>e</i> +01	2.33e+01	1.00e+00	4.55e - 01
8	2.90e+01	2.90e+01	2.20e+01	$9.28e{-01}$	4.22e - 01
9	3.82 <i>e</i> +01	3.80e+01	2.59e+01	$9.51e{-01}$	4.31e - 01
10	3.08 <i>e</i> +01	3.05 <i>e</i> +01	1.76e+01	4.85e - 01	2.19e - 01
11	1.41 <i>e</i> +01	1.40e+01	8.05 <i>e</i> +00	2.03e-01	9.12e - 02
12	1.35e+01	1.34e+01	7.69e+00	$1.92e{-01}$	8.63e - 02
13	4.36e+00	4.33 <i>e</i> +00	2.58e+00	7.88e - 02	3.58e - 02



Table 14 NSE, Re = 100, ROM projection filter, and d = 14: Average CE and average ROM subfilter-scale stress tensor for different r values

r	2	3	4	5	6	7
$\ \boldsymbol{\mathcal{E}}_{\Delta}[u_d]\ _{L^2(L^2)}$ $\ \boldsymbol{\tau}\ _{L^2(L^2)}$	1.01 <i>e</i> -02	1.00 <i>e</i> -02	1.85 <i>e</i> -02	2.39 <i>e</i> -02	2.50 <i>e</i> -02	3.03 <i>e</i> -02
	3.81 <i>e</i> +00	6.05 <i>e</i> -02	1.25 <i>e</i> +00	1.75 <i>e</i> -01	1.43 <i>e</i> +00	4.09 <i>e</i> -02
r $\ \mathcal{E}_{\Delta}[u_d]\ _{L^2(L^2)}$ $\ \tau\ _{L^2(L^2)}$	8	9	10	11	12	13
	2.90 <i>e</i> -02	3.82 <i>e</i> -02	3.08 <i>e</i> -02	1.41 <i>e</i> -02	1.35 <i>e</i> -02	4.36 <i>e</i> -03
	4.24 <i>e</i> -01	8.61 <i>e</i> -02	4.20 <i>e</i> -01	2.44 <i>e</i> -02	1.42 <i>e</i> -01	1.91 <i>e</i> -02

As in Section 5.1.2, we note that the CE displays a non-monotonic behavior with respect to r; we explain this behavior in Section 5.4.

In Table 14, in addition to the CE average, we also list the ROM subfilter-scale stress tensor average for different r values. The CE average is lower than or on the same order as the ROM subfilter-scale stress tensor average. We note, however, that the CE is multiplied by the inverse of the Reynolds number in the ICE-DDC-ROM (47) and the CE-DDC-ROM (50).

Next, we address (Q2), i.e., we investigate whether the CE has a significant effect on ROMs. To this end, we test the DDC-ROM (46), the ICE-DDC-ROM (47), and the CE-DDC-ROM (50). We note that the ICE-DDC-ROM and CE-DDC-ROM include a representation of the Laplacian CE (9), whereas the DDC-ROM does not. For various r and δ values, we list the ROM error, which is computed by using the metric (51), the ROM differential filter (Table 15), and the ROM projection filter (Table 16). We observe that the ICE-DDC-ROM and CE-DDC-ROM errors are generally lower than the DDC-ROM error. This time, however, the improvements in the ICE-DDC-ROM and CE-DDC-ROM are small. This is different from the Burgers equation in Section 5.1, where the ICE-DDC-ROM and CE-DDC-ROM errors were orders of magnitude lower than the DDC-ROM error. Thus, for the Re = 100 case, we conclude that the CE plays only a minor role in ROM development. This

Table 15 NSE, Re = 100, ROM differential filter: Average error in G-ROM, DDC-ROM, ICE-DDC-ROM, and CE-DDC-ROM for different δ and r values

r	δ	G-ROM	DDC-ROM	ICE-DDC-ROM	CE-DDC-ROM
2	1.00e-03	3.41 <i>e</i> -01	3.3368 <i>e</i> -01	2.9718 <i>e</i> -04	3.3368 <i>e</i> -01
2	1.00e - 02	$3.41e{-01}$	$3.3368e{-01}$	2.9627e - 04	$3.3368e{-01}$
3	1.00e - 03	1.10e - 02	$2.2324e{-04}$	$3.2809e{-04}$	2.3673e - 04
3	1.00e - 02	1.10e - 02	2.2324e - 04	$3.2688e{-04}$	$2.3560e{-04}$
4	1.00e - 03	4.29e - 02	4.1966e - 04	3.4675e - 04	4.1425e - 04
4	1.00e - 02	4.29e - 02	4.1966e - 04	3.4762e - 04	4.1447e - 04
5	1.00e - 03	2.33e-02	3.4739e - 04	3.4129e - 04	3.3897e - 04
5	$1.00e{-02}$	2.33e-02	$3.4739e{-04}$	$3.3851e{-04}$	3.3617e - 04



r	G-ROM	DDC-ROM	ICE-DDC-ROM	CE-DDC-ROM
2	3.41 <i>e</i> -01	3.35e-01	2.97 <i>e</i> -04	3.30e-01
3	1.10e - 02	2.23e-04	3.28e-04	2.37e - 04
4	4.29e - 02	4.20e - 04	3.47e - 04	4.14e - 04
5	2.33e-02	3.47e - 04	3.41e - 04	3.39e - 04
6	3.51e - 02	$3.41e{-04}$	3.50e - 04	3.39e - 04
7	4.87e - 03	4.35e - 04	4.19e - 04	4.11e - 04
8	7.19e - 03	4.29e - 04	4.17e - 04	4.13e - 04
9	5.82e - 03	4.34e - 04	4.11e - 04	4.11e - 04
10	7.14e - 03	4.16e - 04	4.13e - 04	4.10e - 04
11	1.52e - 03	4.36e - 04	4.34e - 04	4.33e - 04
12	1.86e - 03	4.42e - 04	4.48e - 04	4.40e - 04
13	1.21e - 03	6.58e - 04	6.83e - 04	6.58e - 04

Table 16 NSE, Re = 100, d = 14, ROM projection filter: Average error in G-ROM, DDC-ROM, ICE-DDC-ROM, and CE-DDC-ROM for different r values

happens because, in this case, the magnitude of the CE multiplied by the inverse of the Reynolds number is lower than the magnitude of the Correction term.

5.2.2 Reynolds number Re = 500

To investigate the effect of the Reynolds number on the results in Section 5.2.1, in this section we consider Re = 500, which corresponds to $v = 2 \times 10^{-4}$ (see [25, 44] for details on the computational setting). To generate the ROM basis, we collect 1501 snapshots, which are the FE solutions at each time step from t = 5 to t = 8 and represent almost seven periods.

To construct the ROM subfilter-scale stress tensor and the CE in the DDC-ROM (46), the ICE-DDC-ROM (47), and the CE-DDC-ROM (50), we use 219 snapshots from the time interval (5, 5.438], which represents approximately one period.

As in Section 5.2.1, we start by addressing (Q1), i.e., we measure the size of the CE. For various r and δ values, we list the CE computed by using the ROM differential filter (Table 17) and the ROM projection filter (Table 18). As in Section 5.2.1, we observe that the CE exists for both filters.

In Table 18, in addition to the CE average, we also list the ROM subfilter-scale stress tensor average for different r values. The CE average is larger than or on the same order as the ROM subfilter-scale stress tensor average. We note, however, that the CE is multiplied by the inverse of the Reynolds number in the ICE-DDC-ROM (47) and the CE-DDC-ROM (50).

Next, we address (Q2), i.e., we investigate whether the CE has a significant effect on ROMs. To this end, we test the DDC-ROM (46), the ICE-DDC-ROM (47), and the CE-DDC-ROM (50). We note that the ICE-DDC-ROM and CE-DDC-ROM include a representation of the Laplacian CE (9), whereas the DDC-ROM does not. For various r and δ values, we list the ROM error, which is computed by using the metric (51),



r	$\delta = 1.00e - 04$	$\delta = 1.00e - 03$	$\delta = 1.00e - 2$	$\delta = 1.00e - 01$	$\delta = 1.50e - 01$
3	5.46e-02	5.44 <i>e</i> -02	5.06e-02	6.40 <i>e</i> -03	3.08e-03
4	2.58e - 02	2.58e - 02	1.96e - 02	1.48e - 03	7.00e-04
5	4.18e - 02	4.16e - 02	3.18e - 02	1.78e - 03	8.30e - 04
6	2.38e - 02	2.36e - 02	1.90e - 02	1.46e - 03	6.86e - 04
7	2.36e - 02	2.34e - 02	1.80e - 02	1.10e - 03	5.14e - 04
8	2.36e - 02	2.36e - 02	1.72e - 02	6.84e - 04	3.12e - 04
9	3.02e-02	3.00e-02	1.62e - 02	5.62e - 04	2.56e - 04
10	3.70e - 02	3.64e - 02	1.64e - 02	4.70e - 04	2.14e - 04

Table 17 NSE, Re = 500, ROM differential filter, d = 20: Average CE for different δ and r values

the ROM differential filter (Table 19), and the ROM projection filter (Table 20). We observe that the ICE-DDC-ROM and CE-DDC-ROM errors are lower than the DDC-ROM error, but the improvements in the ICE-DDC-ROM and CE-DDC-ROM over the DDC-ROM are small, just as in Section 5.2.1. Thus, for the Re = 500 case, we conclude that the CE plays only a minor role in ROM development, just as for the Re = 100 test case in Section 5.2.1. Again, this happens because, in this case, the magnitude of the CE multiplied by the inverse of the Reynolds number is much lower than the magnitude of the Correction term.

5.3 Predictive regime

In the numerical experiments in this section, we considered the *reconstructive regime*. This regime aims at checking whether the tested ROMs can reproduce the dynamics of the underlying system on the time interval $[T_{\min}, T_{\max}]$, which is the *same* time interval as the time interval used to generate the ROM basis functions. Thus, in the reconstructive regime, the ROMs are validated on the same time interval as the time interval used to train the ROMs. Of course, testing the ROMs in the reconstructive regime is a necessary first step in checking the ROM accuracy.

The *predictive regime* is a significantly harder test case than the reconstructive regime. In the predictive regime, the ROMs are trained on a short time interval, e.g., $\left[T_{\min}, \frac{T_{\max}}{2}\right]$, and validated on a longer time interval $\left[T_{\min}, T_{\max}\right]$. In other words, the ROM basis functions are constructed from *incomplete data*, but the ROMs are validated on the entire time interval.

Table 18 NSE, Re = 500, ROM projection filter, and d = 20: Average CE and average ROM subfilter-scale stress tensor for different r values

r	2	3	4	5	6	7
$\ \boldsymbol{\mathcal{E}}_{\Delta}[\boldsymbol{u}_d]\ _{L^2(L^2)}$ $\ \boldsymbol{\tau}\ _{L^2(L^2)}$					2.38 <i>e</i> -02 6.11 <i>e</i> -01	



Table 19 NSE, $Re = 500$, $d = 20$, ROM differential filter: Average error in G-ROM, DDC-ROM,
ICE-DDC-ROM, and CE-DDC-ROM for different δ and r values

r	δ	G-ROM	DDC-ROM	ICE-DDC-ROM	CE-DDC-ROM
2	1.00e-03	7.23e-01	5.16e-01	8.04 <i>e</i> -04	5.16e-01
2	1.00e-02	7.23e-01	5.16e - 01	7.27e - 04	5.16e - 01
3	1.00e-03	8.44e - 02	1.55e - 03	9.70e - 04	1.49e - 03
3	1.00e-02	$8.44e{-02}$	1.55e - 03	9.81e - 04	1.50e - 03
4	1.00e-03	$4.80e{-02}$	1.87e - 03	1.06e - 03	1.86e - 03
4	1.00e - 02	$4.80e{-02}$	1.87e - 03	1.06e - 03	1.86e - 03
5	1.00e-03	1.26e - 01	1.20e - 03	1.08e - 03	1.21e-03
5	$1.00e{-02}$	$1.26e{-01}$	$1.20e{-03}$	1.08e - 03	$1.21e{-03}$

In this section, we perform a numerical investigation of the CE in the predictive regime. In our numerical investigation, we consider two test problems: In Section 5.3.1, we consider the 1D viscous Burgers equation test problem that we used in Section 5.1.1. In Section 5.3.2, we consider the 2D channel flow past a circular cylinder test problem that we used in Section 5.2.2.

5.3.1 Burgers equation, smooth initial condition

In this section, we consider the numerical test in Section 5.1.1. For clarity, we include results only for the ROM projection filter. All the parameters are the same as those used in Section 5.1.1; the only difference is that now we construct the ROMs by using

Table 20 NSE, Re = 500, d = 20, ROM projection filter: Average error in G-ROM, DDC-ROM, ICE-DDC-ROM, and CE-DDC-ROM for different r values

r	G-ROM	DDC-ROM	ICE-DDC-ROM	CE-DDC-ROM
2	7.23 <i>e</i> -01	5.16e-01	3.17 <i>e</i> -03	5.16e-01
3	$8.44e{-02}$	1.55e - 03	8.36e - 04	1.49e - 03
4	$4.80e{-02}$	1.01e - 03	1.02e-03	1.12e-03
5	1.26e - 01	1.20e - 03	1.06e-03	1.21e-03
6	1.50e - 01	1.27e - 03	1.08e - 03	1.24e - 03
7	1.49e - 01	1.49e - 03	1.19e - 03	1.47e - 03
8	2.41e - 02	1.40e - 03	1.52e - 03	1.39e-03
9	2.56e - 02	1.52e - 03	1.52e - 03	1.52e - 03
10	2.36e - 02	1.44e - 03	1.46e - 03	1.44e - 03
11	2.61e - 02	1.44e - 03	1.45e - 03	1.46e - 03
12	1.52e - 02	1.54e - 03	1.44e - 03	1.57e - 03
13	1.55e - 02	1.53e - 03	1.45e - 03	1.53e - 03
14	1.11e - 02	1.51e - 03	1.46e - 03	1.51e - 03



Table 21 Predictive regime; Burgers equation, ROM projection filter, smooth initial condition, $v = 10^{-1}$, and d = 5: Average CE and ROM subfilter-scale stress tensor for different r values

r	$ \mathcal{E}_{\Delta}[u_d] _{L^2(L^2)}$	$ \tau _{L^2(L^2)}$
1	2.9508e - 01	1.8396e - 02
2	2.4307e - 02	9.7433e - 04
3	1.1821e - 03	3.4550e - 05
4	4.4356e - 05	1.0123e - 06

only data from the time interval $\left[T_{\min}, \frac{T_{\max}}{10}\right] = [0, 0.1]$, whereas in Section 5.1.1 we used data on the time interval $\left[T_{\min}, T_{\max}\right] = [0, 1]$. Thus, we train the ROMs on a time interval that is *ten times shorter* than the time interval on which we test the ROMs.

First, we address (Q1), i.e., we measure the size of the CE. In Table 21, for various r values, we list the magnitude of the CE together with the magnitude of the ROM subfilter-scale stress tensor. The main conclusion is that, for all r values, the CE exists. Furthermore, the CE average dominates the ROM subfilter-scale stress tensor average. We also observe that, as expected, as r increases, the magnitudes of the averages of the CE and the ROM subfilter-scale stress tensor decrease.

Next, we address (Q2), i.e., we investigate whether the CE has a significant effect on ROMs. To this end, we test the DDC-ROM (46), the ICE-DDC-ROM (47), and the CE-DDC-ROM (50). We note again that the ICE-DDC-ROM and CE-DDC-ROM include a representation of the Laplacian CE (9), whereas the DDC-ROM does not. In Table 22, for various r values, we list the ROM error, which is computed by using the metric (51). We observe that the CE-DDC-ROM errors are consistently lower than the DDC-ROM error (which, in turn, are lower than the G-ROM errors). We emphasize that, for r=2,3,4, the CE-DDC-ROM errors are one and even two orders of magnitude lower than the DDC-ROM errors. Thus, we conclude that the CE plays a significant role in ROM development. Table 22 also shows that the CE-DDC-ROM errors are significantly lower than the ICE-DDC-ROM errors. We note, however, that this does not contradict the nature of the ICE-DDC-ROM, which is ideal only on the training interval (i.e., [0, 0.1]), but not on the entire testing interval (i.e., [0, 1]).

The results in Tables 21 and 22 obtained in the predictive regime are similar to those obtained in Section 5.1.1 for the reconstructive regime: The CE is relatively

Table 22 Predictive regime; Burgers equation, ROM projection filter, smooth initial condition, $\nu=10^{-1}$, and d=5: Average error in G-ROM, DDC-ROM, ICE-DDC-ROM, and CE-DDC-ROM for different r values

r	G-ROM	DDC-ROM	ICE-DDC-ROM	CE-DDC-ROM
1	4.0154e - 02	2.0314e - 02	2.0194e - 02	1.3837e - 02
2	1.1492e - 02	8.4462e - 03	8.4463e - 03	8.2671e - 04
3	3.3987e - 03	2.8191e - 03	2.8191e - 03	1.7522e - 05
4	1.0226e - 03	4.8016e - 04	4.8016e - 04	2.7080e - 05



large and the ROMs that model the CE are significantly more accurate than the ROMs that do not model the CE.

5.3.2 Channel flow past a circular cylinder, Re = 500

In this section, we consider the numerical test in Section 5.2.2. For clarity, we include results only for the ROM projection filter. All the parameters are the same as those used in Section 5.2.2; the only difference is that now we construct the ROM basis and ROMs by using only data from the time interval [5, 5.3], whereas in Section 5.2.2 we used data from the time interval [5, 8] for the ROM basis and data from the time interval (5, 5.438] for the ROMs. Thus, we train the ROMs on a time interval that is *ten times shorter* than the time interval on which we test the ROMs.

We investigate whether the CE has a significant effect on ROMs. To this end, we test the DDC-ROM (46), the ICE-DDC-ROM (47), and the CE-DDC-ROM (50). We note again that the ICE-DDC-ROM and CE-DDC-ROM include a representation of the Laplacian CE (9), whereas the DDC-ROM does not. Tables 23 and 24 list the ROM error computed by using the metrics (51) and (57), respectively. We observe that the ICE-DDC-ROM and CE-DDC-ROM errors are similar to the DDC-ROM error, just as in the reproductive case in Section 5.2.2. Thus, for the Re = 500 case, we conclude that the CE plays only a minor role in ROM development, just as in the reproductive case in Section 5.2.2. Again, this happens because, in this case, the magnitude of the CE multiplied by the inverse of the Reynolds number is lower than the magnitude of the Correction term. Table 23 also shows that the CE-DDC-ROM errors are generally lower than the ICE-DDC-ROM errors. We note, however, that this does not contradict the nature of the ICE-DDC-ROM, which is ideal only on the training interval (i.e., [5, 5.3]), but not on the entire testing interval (i.e., [5, 8]).

Table 23 Predictive regime; NSE, ROM projection filter, Re=500, and d=20: Average error computed by using metric (51) for G-ROM, DDC-ROM, ICE-DDC-ROM, and CE-DDC-ROM for different r values

r	G-ROM	DDC-ROM	ICE-DDC-ROM	CE-DDC-ROM
2	2.97e-01	9.26e-03	7.23e-03	8.64e-03
3	3.68e-01	1.03e-01	1.98e-01	1.04e-01
4	3.39e-01	5.78e-03	5.79e-03	5.55e-03
5	3.79e-01	1.17e-01	1.95e-01	1.18e-01
6	6.54e - 02	3.29e-03	3.69e-03	3.41e-03
7	5.87e-02	1.97e-02	3.00e-02	1.99e-02
8	5.29e-02	2.80e-03	2.86e-03	2.80e-03
9	5.92e - 02	1.75e-02	3.12e-02	1.77e-02
10	3.49e - 02	2.55e-03	2.76e-03	2.57e-03
11	3.22e-02	9.63e-03	1.54e - 02	9.57e-03
12	2.18e - 02	2.34e-03	2.33e-03	2.34e - 03
13	2.22e-02	5.92e-03	1.12e-02	5.92e-03
14	1.01e-02	2.00e-03	2.02e-03	2.02e-03



Table 24 Predictive regime; NSE, ROM projection filter, Re=500, and d=20: Average error computed by using metric (57) for G-ROM, DDC-ROM, ICE-DDC-ROM, and CE-DDC-ROM for different r values

r	G-ROM	DDC-ROM	ICE-DDC-ROM	CE-DDC-ROM
2	3.42e-01	1.42e-01	1.41e-01	1.42e-01
3	3.91e-01	1.56e-01	2.33e-01	1.57e-01
4	3.51e-01	7.90e-02	7.89e-02	7.89e - 02
5	3.86e-01	1.34e-01	2.05e-01	1.35e-01
6	7.52e-02	3.47e-02	3.47e-02	3.47e-02
7	6.66e - 02	3.63e-02	4.29e-02	3.64e - 02
8	5.93e-02	2.52e-02	2.52e-02	2.52e-02
9	6.32e - 02	2.75e-02	3.79e-02	2.76e-02
10	3.85e-02	1.54e-02	1.54e - 02	1.54e - 02
11	3.51e-02	1.65e-02	2.05e-02	1.64e - 02
12	2.47e-02	1.12e-02	1.12e-02	1.12e-02
13	2.43e-02	1.12e-02	1.47e-02	1.12e-02
14	1.24e-02	7.49e-03	7.50e-03	7.49e - 03

5.4 Rates of convergence

In the numerical experiments in this section, we used formula (51) to compute the ROM error as the difference between the ROM approximation and the DNS solution projected onto the ROM space X^r , which is the space spanned by the first r ROM basis functions: $X^r = \text{span}\{\phi_1, \phi_2, \cdots, \phi_r\}$. Since the second term in the ROM error formula (51) (i.e., $\sum_{i=1}^r \left(u^{DNS}, \phi_i\right) \phi_i$), changes when r changes, in some of the tables in this section, the ROM error did not display monotonic convergence with respect to r.

We believe that the ROM error formula (51) is appropriate to quantify the ROM accuracy since, for a fixed r value, it measures the distance between the ROM solution and the best approximation in the ROM space X^r . If, however, the goal is to illustrate monotonic convergence with respect to r, the following formula seems more appropriate:

$$\left\| \boldsymbol{u}_r - \sum_{i=1}^d \left(\boldsymbol{u}^{DNS}, \boldsymbol{\phi}_i \right) \boldsymbol{\phi}_i \right\|, \tag{57}$$

where u_r is the ROM approximation and u^{DNS} is the DNS solution. The difference between formula (57) and formula (51) is that the sum in the former goes from 1 to d, whereas in the latter it goes from 1 to r. Thus, in formula (57), the ROM error is computed as the difference between the ROM approximation and the DNS solution projected onto the ROM space X^d , which is the space spanned by the first d ROM basis functions: $X^d = \text{span}\{\phi_1, \phi_2, \cdots, \phi_d\}$. Since the second term in the ROM error formula (57) (i.e., $\sum_{i=1}^{d} (u^{DNS}, \phi_i) \phi_i$) does not change with respect to r, we expect the ROM error computed with (57) to display monotonic convergence with



respect to r. Next, we show that this is indeed the case for the test problems used in Sections 5.1.1 and 5.2.2 in the reconstructive regime.

First, we consider the test problem in Section 5.1.1. We use the same parameters as those used in Section 5.1.1, except that we choose $\nu=1$ and d=9. In Table 25, we list the average ROM errors for the G-ROM (38), the DDC-ROM (46), the ICE-DDC-ROM (47), and the CE-DDC-ROM (50) computed with formula (57). In Table 26, we list the rates of convergence corresponding to these errors. As expected, all the ROM errors in Tables 25 converge monotonically with respect to r. This is clearly displayed in Table 26, where all the numerical rates of convergence are very close to the theoretical rates of convergence [22] (i.e., close to 1).

Next, we consider the test problem in Section 5.2.2. We use the same parameters as those used in Section 5.2.2. In Table 27, we list the average ROM errors for the G-ROM (38), the DDC-ROM (46), the ICE-DDC-ROM (47), and the CE-DDC-ROM (50) computed with formula (57). Again, almost all the ROM errors in Table 27 converge asymptotically with respect to r.

In Table 26, we use the following formula to compute the rate of convergence (ROC) [17, 18]:

$$ROC(r) = \frac{\log(E(r)) - \log(E(r-1))}{\log(\Lambda(r)) - \log(\Lambda(r-1))} \quad r = 2, ..., d-1,$$
 (58)

where E represents the ROM error (for the G-ROM, DDC-ROM, ICE-DDC-ROM, and CE-DDC-ROM) and $\Lambda = \sqrt{\frac{1}{M}\sum_{i=r+1}^{d}\lambda_i}$ represents the POD truncation error.

We note, however, that in Tables 25 and 27, the improvements in the CE-DDC-ROM, ICE-DDC-ROM, and DDC-ROM errors over the G-ROM error are much smaller than the corresponding improvements in Sections 5.1.1 and 5.2.2. The reason

Table 25 Burgers equation, ROM projection filter, smooth initial condition, v = 1, and d = 9: Average error in G-ROM, DDC-ROM, ICE-DDC-ROM, and CE-DDC-ROM for different r values computed with formula (57)

G-ROM	DDC-ROM	ICE-DDC-ROM	CE-DDC-ROM
1.5142e - 01	1.4047e - 01	1.2669e - 01	1.2829e - 01
2.0326e - 02	1.9058e - 02	1.6665e - 02	1.6665e - 02
2.7029e - 03	2.5604e - 03	2.2314e - 03	2.2314e - 03
3.6104e - 04	3.2263e - 04	3.0067e - 04	3.0067e - 04
4.8384e - 05	4.1544e - 05	4.0587e - 05	4.0587e - 05
6.4558e - 06	5.8634e - 06	5.4464e - 06	5.4464e - 06
8.5465e - 07	7.9244e - 07	7.2401e - 07	7.2401e - 07
1.1363e - 07	1.1018e - 07	9.6637e - 08	9.6623e - 08
	1.5142e - 01 $2.0326e - 02$ $2.7029e - 03$ $3.6104e - 04$ $4.8384e - 05$ $6.4558e - 06$ $8.5465e - 07$	$\begin{array}{cccccccccccccccccccccccccccccccccccc$	$\begin{array}{cccccccccccccccccccccccccccccccccccc$



Table 26 Burgers equation, ROM projection filter, smooth initial condition, v = 1, and d = 9: Rates of convergence of G-ROM, DDC-ROM, ICE-DDC-ROM, and CE-DDC-ROM for different r values computed with formula (57)

r	$\sqrt{\frac{1}{M}\sum_{i=r+1}^{d}\lambda_i}$	G-ROM	DDC-ROM	ICE-DDC-ROM	CE-DDC-ROM
1	3.9643e - 03	_	_	_	_
2	5.2666e - 04	9.9486e - 01	9.8959e - 01	1.0049e + 00	1.0111e + 00
3	7.0529e - 05	1.0035e + 00	9.9840e - 01	1.0001e + 00	1.0001e + 00
4	9.5032e - 06	1.0043e + 00	1.0334e + 00	9.9999e - 01	9.9999e - 01
5	1.2828e - 06	1.0036e + 00	1.0236e + 00	9.9999e - 01	9.9999e - 01
6	1.7214e - 07	1.0028e + 00	9.7487e - 01	1.0000e + 00	1.0000e + 00
7	2.2879e - 08	1.0020e + 00	9.9171e - 01	9.9991e - 01	9.9991e - 01
8	3.0123e - 09	9.9518e - 01	9.7311 <i>e</i> – 01	9.9326e - 01	9.9332e - 01

for this behavior can be seen by applying the triangle inequality to the ROM error formula (57)

$$\left\| \boldsymbol{u}_{r} - \sum_{i=1}^{d} \left(\boldsymbol{u}^{DNS}, \boldsymbol{\phi}_{i} \right) \boldsymbol{\phi}_{i} \right\| \leq \left\| \boldsymbol{u}_{r} - \sum_{i=1}^{r} \left(\boldsymbol{u}^{DNS}, \boldsymbol{\phi}_{i} \right) \boldsymbol{\phi}_{i} \right\| + \left\| \sum_{i=r+1}^{d} \left(\boldsymbol{u}^{DNS}, \boldsymbol{\phi}_{i} \right) \boldsymbol{\phi}_{i} \right\|$$

$$(59)$$

Table 27 NSE, Re = 500, d = 20, ROM projection filter: Average error in G-ROM, DDC-ROM, ICE-DDC-ROM, and CE-DDC-ROM for different r values computed with formula (57)

r	G-ROM	DDC-ROM	ICE-DDC-ROM	CE-DDC-ROM
2	3.35e-01	1.41e-01	1.41e-01	1.41e-01
3	3.60e-01	1.42e-01	1.96e - 01	1.42e-01
4	3.60e-01	7.85e-02	7.84e - 02	7.85e-02
5	3.86e-01	9.32e-02	2.03e-01	9.41e-02
6	7.32e-02	3.45e-02	3.47e - 02	3.45e-02
7	6.52e-02	3.50e-02	4.17e-02	3.48e - 02
8	5.96e-02	2.54e-02	2.56e-02	2.54e-02
9	6.41e - 02	2.69e-02	3.75e-02	2.69e - 02
10	3.84e - 02	1.49e-02	1.49e - 02	1.49e - 02
11	3.44e - 02	1.51e-02	1.92e-02	1.50e-02
12	2.32e-02	1.06e-02	1.06e-02	1.06e-02
13	2.27e-02	1.02e-02	1.36e-02	1.02e-02
14	1.21e-02	6.60e-03	6.60e-03	6.59e-03



and noticing that the last term in (59) (i.e., the ROM truncation error) dominates the second term in (59) (i.e., the ROM error in (51) used in Sections 5.1.1 and 5.2.2).

We emphasize, however, that the numerical tests that we used in this section are relatively simple. Furthermore, as we noted before, in this paper we did *not* focus on the development of ROM closure models. Instead, we aimed at discovering *all* the components that are needed to assemble the "correct" ROM closure model. The numerical results suggest that, for the metrics used in this paper, the CE could be a significant component of ROM closure models. Of course, in future studies we will investigate ROM closure models that integrate all the components (i.e., the ROM subfilter-scale stress tensor, the ROM CE, and physical constraints [25]) and will test them in challenging, realistic computational settings [30, 42].

Finally, we present results for the relative ROM error:

$$\frac{\left\|\boldsymbol{u}_{r} - \sum_{i=1}^{d} \left(\boldsymbol{u}^{DNS}, \boldsymbol{\phi}_{i}\right) \boldsymbol{\phi}_{i}\right\|}{\left\|\sum_{i=1}^{d} \left(\boldsymbol{u}^{DNS}, \boldsymbol{\phi}_{i}\right) \boldsymbol{\phi}_{i}\right\|},$$
(60)

where u_r is the ROM approximation and u^{DNS} is the DNS solution.

For clarity, we consider only the test problem in Section 5.1.1 and the ROM projection filter. We use the same parameters as those used in Section 5.1.1, except that we choose $\nu=1$ and d=9. In Table 28, we list the relative ROM errors for the G-ROM, the DDC-ROM, the ICE-DDC-ROM, and the CE-DDC-ROM computed with formula (60).

The results in Table 28 obtained for the relative error are qualitatively similar to the results obtained in Tables 25 and 27 for the absolute error: The improvements in the CE-DDC-ROM, ICE-DDC-ROM, and DDC-ROM errors over the G-ROM error are much smaller than the corresponding improvements in Section 5.1.1.

Table 28 Burgers equation, L^2 -POD, ROM projection filter, smooth initial condition, v=1, and d=9: Relative error in G-ROM, DDC-ROM, ICE-DDC-ROM, and CE-DDC-ROM for different r values computed with formula (60)

r	G-ROM	DDC-ROM	ICE-DDC-ROM	CE-DDC-ROM
1	1.5842e - 01	1.4696e — 01	1.3255e - 01	1.3422e - 01
2	2.1265e - 02	1.9938e - 02	1.7435e - 02	1.7435e - 02
3	2.8278e - 03	2.6788e - 03	2.3346e - 03	2.3346e - 03
4	3.7773e - 04	3.3754e - 04	3.1456e - 04	3.1456e - 04
5	5.0620e - 05	4.3453e - 05	4.2462e - 05	4.2462e - 05
6	6.7542e - 06	6.1344e - 06	5.6981e - 06	5.6981e - 06
7	8.9415e - 07	8.2907e - 07	7.5747e - 07	7.5747e - 07
8	1.1889e - 07	1.1527e - 07	1.0110e - 07	1.0100e - 07



5.5 ROM basis

Both in the ROM basis construction and in the numerical investigation of the CE, we used the L^2 norm, $\|\cdot\|$, defined on the space $X:=H^1_0(\Omega)$. We note, however, that we could use different norms, e.g., the H^1_0 norm $\|\mathbf{v}\|_{H^1_0}:=\|\nabla\mathbf{v}\|$ and its corresponding inner product $(\mathbf{u},\mathbf{v})_{H^1_0}:=(\nabla\mathbf{u},\nabla\mathbf{v})$. The ROM basis constructed using the H^1_0 norm is different from the ROM basis built using the L^2 norm. Similarly, using the the H^1_0 norm instead of the L^2 norm has an effect on the CE, since the ROM mass matrix, $M_r=(\phi_i,\phi_j)$, i,j=1,...,r, and the ROM stiffness matrix, $S_r=(\nabla\phi_i,\nabla\phi_j)$, i,j=1,...,r, have different forms.

In this section, we investigate numerically the CE for the projection filter and the H_0^1 norm and inner product in the reconstructive regime. For simplicity, we use the H_0^1 norm and inner product only to generate the ROM basis. To derive the CE, we use the L^2 norm and inner product, just as we did in Section 3.4 (using the H_0^1 norm and inner product to derive the CE would require the use of higher order FEs). We consider the same test problem as that used in Section 5.1.1, but with $\nu=1$ and d=9. We build the ROM basis by using the POD approach described in Section 2, but with the H_0^1 inner product instead of the L^2 inner product. Furthermore, we use the same derivation of the CE as that used in Section 3.4, but with the ROM mass matrix, M_r , and the ROM stiffness matrix, S_r , built with the H_0^1 ROM basis.

First, we address (Q1), i.e., we measure the size of the CE. In Table 29, for various r values, we list the magnitude of the CE together with the magnitude of the ROM subfilter-scale stress tensor. The main conclusion is that, for all r values, the CE exists. Furthermore, the CE average dominates the ROM subfilter-scale stress tensor average. We also observe that, as expected, as r increases, the magnitudes of the averages of the CE and the ROM subfilter-scale stress tensor decrease.

Next, we address (Q2), i.e., we investigate whether the CE has a significant effect on ROMs. To this end, we test the DDC-ROM (46), the ICE-DDC-ROM (47), and the CE-DDC-ROM (50). We note again that the ICE-DDC-ROM and CE-DDC-ROM include a representation of the Laplacian CE (9), whereas the DDC-ROM does not.

Table 29 H	H_0^1 ROM basis; Burgers equation, ROM projection filter, smooth initial condition, $\nu = 1$, and
d = 9: Aver	rage CE and ROM subfilter-scale stress tensor for different r values

r	$ \mathcal{E}_{\Delta}[u_d] _{L^2(L^2)}$	$ au _{L^2(L^2)}$	
1	4.7667e - 01	1.8613e - 03	
2	1.5660e - 01	9.6419e - 05	
3	3.2568e - 02	6.4306e - 06	
4	5.5176e - 03	4.7886e - 07	
5	8.3244e - 04	3.7957e - 08	
6	1.1579e - 04	3.1112e - 09	
7	1.4949e - 05	2.5525e - 10	
8	1.8482e - 06	2.0374e - 11	



7.6664e - 08

7.6666e - 08

r	G-ROM	DDC-ROM	ICE-DDC-ROM	CE-DDC-ROM
1	1.2643e - 02	9.1244e - 03	1.1745e - 03	1.3460e - 03
2	1.8191e - 03	1.3926e - 03	1.4379e - 05	1.4669e - 05
3	1.9644e - 04	1.6081e - 04	1.5983e - 07	1.4209e - 07
4	2.0358e - 05	7.3515e - 06	7.6074e - 08	7.6990e - 08
5	2.0651e - 06	7.3785e - 07	7.6377e - 08	7.6577e - 08
6	2.1943e - 07	1.6302e - 07	7.6560e - 08	7.6681e - 08

7.6662e - 08

7.6666e - 08

7.8591e - 08

7.6685e - 08

Table 30 H_0^1 ROM basis; Burgers equation, ROM projection filter, smooth initial condition, $\nu=1$, and d=9: Average error in G-ROM, DDC-ROM, ICE-DDC-ROM, and CE-DDC-ROM for different r values

In Table 30, for various r values, we list the ROM error calculated with formula (51). We observe that the CE-DDC-ROM errors are consistently lower than the DDC-ROM error (which, in turn, are lower than the G-ROM errors). We emphasize that, for r = 2, 3, 4, the CE-DDC-ROM errors are *one and even two orders of magnitude* lower than the DDC-ROM errors. Thus, we conclude that the CE plays a significant role in ROM development.

The results in Tables 29 and 30 obtained for the H_0^1 ROM basis are similar to those obtained in Section 5.1.1 for the L^2 ROM basis: The CE is relatively large and the ROMs that model the CE are significantly more accurate than the ROMs that do not model the CE.

6 Conclusions and future work

7.9222e - 08

7.6690e - 08

In this paper, we investigated theoretically and computationally whether the commutation error (CE) exists, i.e., whether differentiation and ROM spatial filtering commute. To our knowledge, this is the first investigation of the CE in a ROM context. We studied whether there is a CE for the Laplacian for two ROM filters: the ROM projection and the ROM differential filter. Furthermore, when the CE was nonzero, we investigated whether it had any significant effect on the ROM development. To this end, we considered the data-driven correction ROM (DDC-ROM) [44], in which the Correction term (which is generally added to improve the ROM's accuracy) is modeled by using the available data. To investigate the effect of the CE on the DDC-ROM, we considered the commutation error DDC-ROM (CE-DDC-ROM), in which available data is used to model not only the Correction term, but also the CE. Finally, we also used the ideal CE-DDC-ROM (ICE-DDC-ROM), which is the DDC-ROM supplemented with a fine resolution representation of the CE. When the CE-DDC-ROM and ICE-DDC-ROM yielded more accurate results than the standard DDC-ROM, we concluded that, when the metric (51) is used, the CE has a significant effect on the ROM development. As numerical tests, we used the Burgers equation with viscosities $\nu = 10^{-1}$ and $\nu = 10^{-3}$ and a 2D flow past a circular cylinder at



7

8

Reynolds numbers Re = 100 and Re = 500. For the Burgers equation test case, we considered smooth and non-smooth initial conditions.

The most important conclusions of our theoretical and numerical investigation that used the metric (51) are the following: (i) The CE exists for all cases considered. (ii) The CE has a significant effect on the ROM development for low Reynolds numbers, but not so much for higher Reynolds numbers. This happens because, for higher Reynolds numbers, the CE (which arises from the diffusion term) is dominated by the Correction term (which arises from the nonlinear term). We note that, for the Burgers equation, the CE had a significant effect on ROMs even for low viscosity values; however, for non-smooth initial conditions (results not included), the CE effect was lower than the CE effect for higher viscosity. (iii) The non-smooth initial conditions (in the Burgers equation) decreased the effect of the CE on the ROM development.

These first steps in the theoretical and numerical investigation of the CE showed that, in some cases, it can be significant and has to be modeled. There are, however, several other research directions that need to be pursued for a better understanding of the ROM CE. For example, we plan to investigate whether there is an upper bound for the Reynolds number for which the CE has a significant effect on the ROM. We also plan to use alternative metrics to compute the ROM error and study their effect on the conclusions of this CE investigation. Furthermore, we plan to study the ROM CE for differential operators that are different from the Laplacian, e.g., first-order spatial derivatives, such as those in the quasi-geostrophic equations. The effect of the CE on 3D complex flows also needs to be studied. Finally, we plan to investigate whether the CE has a significant effect on spatially-filtered ROMs that are different from the DDC-ROM considered in this paper, e.g., the physically constrained data-driven ROM [25] or the approximate deconvolution ROM [45].

Acknowledgements We thank the three anonymous reviewers for their constructive comments and suggestions, which significantly improved the manuscript.

References

- Baiges, J., Codina, R., Idelsohn, S.: Reduced-order subscales for POD models. Comput. Methods Appl. Mech. Engrg. 291, 173–196 (2015)
- 2. Ballarin, F., Manzoni, A., Quarteroni, A., Rozza, G.: Supremizer stabilization of POD–galerkin approximation of parametrized steady incompressible Navier–Stokes equations. Int. J. Numer. Meth. Engng. **102**, 1136–1161 (2015)
- 3. Benosman, M., Borggaard, J., San, O., Kramer, B.: Learning-based robust stabilization for reduced-order models of 2D and 3D Boussinesq equations. Appl. Math. Model. 49, 162–181 (2017)
- Bergmann, M., Ferrero, A., Iollo, A., Lombardi, E., Scardigli, A., Telib, H.: A zonal Galerkin-free POD model for incompressible flows. J. Comput. Phys. 352, 301–325 (2018)
- Berselli, L.C., Iliescu, T., Layton, W.J.: Mathematics of large eddy simulation of turbulent flows. Scientific Computation. Springer, Berlin (2006)
- Brenner, S., Scott, R.: The mathematical theory of finite element methods, vol. 15. Springer, Berlin (2007)
- 7. Brunton, S.L., Proctor, J.L., Kutz, J.N.: Discovering governing equations from data by sparse identification of nonlinear dynamical systems. Proc. Natl. Acad. Sci. 113(15), 3932–3937 (2016)
- Carlberg, K., Barone, M., Antil, H.: Galerkin v. least-squares Petrov–Galerkin projection in nonlinear model reduction. J. Comput. Phys. 330, 693–734 (2017)



- Couplet, M., Sagaut, P., Basdevant, C.: Intermodal energy transfers in a proper orthogonal decomposition—Galerkin representation of a turbulent separated flow. J. Fluid Mech. 491, 275–284 (2003)
- Fareed, H., Singler, J.R.: A note on incremental pod algorithms for continuous time data. Appl. Numer. Math. (2019)
- 11. Feppon, F., Lermusiaux, P.F.J.: Dynamically orthogonal numerical schemes for efficient stochastic advection and Lagrangian transport. SIAM Rev. 60(3), 595–625 (2018)
- Fick, L., Maday, Y., Patera, A.T., Taddei, T.: A stabilized POD model for turbulent flows over a range of Reynolds numbers: optimal parameter sampling and constrained projection. J. Comp. Phys. 371, 214–243 (2018)
- Gouasmi, A., Parish, E.J., Duraisamy, K.: A priori estimation of memory effects in reduced-order models of nonlinear systems using the Mori–Zwanzig formalism. Proc. R. Soc. A 473(2205), 20170385 (2017)
- Gunzburger, M., Jiang, N., Schneier, M.: An ensemble-proper orthogonal decomposition method for the nonstationary Navier-Stokes equations. SIAM J. Numer. Anal. 55(1), 286–304 (2017)
- 15. Hesthaven, J.S., Rozza, G., Stamm, B.: Certified reduced basis methods for parametrized partial differential equations. Springer, Berlin (2015)
- Holmes, P., Lumley, J.L., Berkooz, G.: Turbulence, coherent structures, dynamical systems and symmetry. Cambridge (1996)
- 17. Iliescu, T., Wang, Z.: Are the snapshot difference quotients needed in the proper orthogonal decomposition? SIAM J. Sci. Comput. 36(3), A1221–A1250 (2014)
- Iliescu, T., Wang, Z.: Variational multiscale proper orthogonal decomposition: Navier-Stokes equations. Num. Meth. P.D.E.s 30(2), 641–663 (2014)
- John, V.: Reference values for drag and lift of a two dimensional time-dependent flow around a cylinder. Int. J. Num. Meth. Fluids 44, 777–788 (2004)
- 20. John, V., Linke, A., Merdon, C., Neilan, M., Rebholz, L.G.: On the divergence constraint in mixed finite element methods for incompressible flows. SIAM Rev. (2016)
- Kondrashov, D., Chekroun, M.D., Ghil, M.: Data-driven non-Markovian closure models. Phys. D 297, 33–55 (2015)
- Kunisch, K., Volkwein, S.: Galerkin proper orthogonal decomposition methods for parabolic problems. Numer. Math. 90(1), 117–148 (2001)
- Loiseau, J.C., Brunton, S.L.: Constrained sparse Galerkin regression. J. Fluid Mech. 838, 42–67 (2018)
- Lu, F., Lin, K.K., Chorin, A.J.: Data-based stochastic model reduction for the Kuramoto–Sivashinsky equation. Phys. D 340, 46–57 (2017)
- Mohebujjaman, M., Rebholz, L.G., Iliescu, T.: Physically-constrained data-driven correction for reduced order modeling of fluid flows. Int. J. Num. Meth. Fluids 89(3), 103–122 (2019)
- Mohebujjaman, M., Rebholz, L.G., Xie, X., Iliescu, T.: Energy balance and mass conservation in reduced order models of fluid flows. J. Comput. Phys. 346, 262–277 (2017)
- Noack, B.R., Morzynski, M., Tadmor, G.: Reduced-order modelling for flow control, vol. 528 Springer Verlag (2011)
- Noack, B.R., Schlegel, M., Ahlborn, B., Mutschke, G., Morzynski, M., Comte, P., Tadmor, G.: A finite-time thermodynamics of unsteady fluid flows. J. Non-Equil. Thermody. 33(2), 103–148 (2008)
- Oberai, A.A., Jagalur-Mohan, J.: Approximate optimal projection for reduced-order models. Int. J. Num. Meth. Engng. 105(1), 63–80 (2016)
- Östh, J., Noack, B.R., Krajnović, S., Barros, D., Borée, J.: On the need for a nonlinear subscale turbulence term in POD models as exemplified for a high-Reynolds-number flow over an Ahmed body. J. Fluid Mech. 747, 518–544 (2014)
- 31. Pan, S., Duraisamy, K.: Data-driven discovery of closure models. SIAM J. Appl. Dyn. Syst. 17(4), 2381–2413 (2018)
- Peherstorfer, B., Willcox, K.: Data-driven operator inference for nonintrusive projection-based model reduction. Comput. Methods Appl. Mech. Engrg. 306, 196–215 (2016)
- Protas, B., Noack, B.R., Östh, J.: Optimal nonlinear eddy viscosity in Galerkin models of turbulent flows. J. Fluid Mech. 766, 337–367 (2015)
- 34. Quarteroni, A., Manzoni, A., Negri, F.: Reduced basis methods for partial differential equations: an introduction, vol. 92 Springer (2015)



- 35. Rebholz, L., Xiao, M.: Improved accuracy in algebraic splitting methods for Navier-Stokes equations. SIAM J. Sci. Comput. **39**(4), A1489–A1513 (2017)
- Rebollo, T.C., Avila, E.D., Mármol, M.G., Ballarin, F., Rozza, G.: On a certified Smagorinsky reduced basis turbulence model. SIAM J. Numer. Anal. 55(6), 3047–3067 (2017)
- San, O., Maulik, R.: Neural network closures for nonlinear model order reduction. Adv. Comput. Math. 44(6), 1717–1750 (2018)
- Schmid, P.J.: Dynamic mode decomposition of numerical and experimental data. J. Fluid Mech. 656, 5–28 (2010)
- 39. Stabile, G., Rozza, G.: Finite volume POD-galerkin stabilised reduced order methods for the parametrised incompressible Navier-Stokes equations. Comput. & Fluids 173, 273–284 (2018)
- Strazzullo, M., Ballarin, F., Mosetti, R., Rozza, G.: Model reduction for parametrized optimal control problems in environmental marine sciences and engineering. SIAM J. Sci. Comput. 40(4), B1055– B1079 (2018)
- Taira, K., Brunton, S.L., Dawson, S., Rowley, C.W., Colonius, T., McKeon, B.J., Schmidt, O.T., Gordeyev, S., Theofilis, V., Ukeiley, L.S.: Modal analysis of fluid flows: an overview. AIAA J.: 4013–4041 (2017)
- 42. Wang, Z., Akhtar, I., Borggaard, J., Iliescu, T.: Proper orthogonal decomposition closure models for turbulent flows: a numerical comparison. Comput. Meth. Appl. Mech. Eng. 237-240, 10–26 (2012)
- Wells, D., Wang, Z., Xie, X., Iliescu, T.: An evolve-then-filter regularized reduced order model for convection-dominated flows. Int. J. Num. Meth. Fluids 84, 598–615 (2017)
- Xie, X., Mohebujjaman, M., Rebholz, L.G., Iliescu, T.: Data-driven filtered reduced order modeling of fluid flows. SIAM J. Sci. Comput. 40(3), B834–B857 (2018)
- 45. Xie, X., Wells, D., Wang, Z., Iliescu, T.: Approximate deconvolution reduced order modeling. Comput. Methods Appl. Mech. Engrg. 313, 512–534 (2017)

Publisher's note Springer Nature remains neutral with regard to jurisdictional claims in published maps and institutional affiliations.

Affiliations

Birgul Koc¹ · Muhammad Mohebujjaman² · Changhong Mou¹ · Traian Iliescu¹

Muhammad Mohebujjaman jaman@psfc.mit.edu

Changhong Mou cmou@vt.edu

Traian Iliescu iliescu@vt.edu

- Department of Mathematics, Virginia Tech, Blacksburg, VA 24061, USA
- Plasma Science and Fusion Center, Massachusetts Institute of Technology, Cambridge, MA 02139, USA

